Title

Vapor–liquid partitioning of alkaline earth and transition metals in NaCl-dominated hydrothermal fluids: An experimental study from 360 to 465°C, near-critical to halite saturated conditions

Authors

Pester, Nicholas J
Ding, Kang
Seyfried, William E

Publication Date

2015-11-01

DOI

10.1016/j.gca.2015.07.028

Peer reviewed

Available online at www.sciencedirect.com

ScienceDirect

Geochimica et Cosmochimica Acta 168 (2015) 111–132

Geochimica et Cosmochimica Acta

www.elsevier.com/locate/gca

Vapor–liquid partitioning of alkaline earth and transition metals in NaCl-dominated hydrothermal fluids: An experimental study from 360 to 465 °C, near-critical to halite saturated conditions

Nicholas J. Pester [a,b,*], Kang Ding [a], William E. Seyfried Jr. [a]

[a] Dept. of Earth Sciences, University of Minnesota, 310 Pillsbury Drive, S.E., Minneapolis, MN 55455, USA
[b] Earth Sciences Division, Lawrence Berkeley National Laboratory, One Cyclotron Road, Berkeley, CA 94720, USA

Received 4 November 2014; accepted in revised form 20 July 2015; available online 26 July 2015

Abstract

Multi-phase fluid flow is a common occurrence in magmatic hydrothermal systems; and extensive modeling efforts using currently established *P–V–T–x* properties of the NaCl–H_2O system are impending. We have therefore performed hydrothermal flow experiments (360–465 °C) to observe vapor–liquid partitioning of alkaline earth and first row transition metals in NaCl-dominated source solutions. The data allow extraction of partition coefficients related to the intrinsic changes in both chlorinity and density along the two-phase solvus. The coefficients yield an overall decrease in vapor affinity in the order Cu(I) > Na > Fe(II) > Zn > Ni(II) ≥ Mg ≥ Mn(II) > Co(II) > Ca > Sr > Ba, distinguished with 95% confidence for vapor densities greater than ~0.2 g/cm^3. The alkaline earth metals are limited to purely electrostatic interactions with Cl ligands, resulting in an excellent linear correlation ($R^2 > 0.99$) between their partition coefficients and respective ionic radii. Though broadly consistent with this relationship, relative behavior of the transition metals is not well resolved, being likely obscured by complex bonding processes and the potential participation of Na in the formation of tetra-chloro species. At lower densities (at/near halite saturation) partitioning behavior of all metals becomes highly non-linear, where *M*/Cl ratios in the vapor begin to increase despite continued decreases in chlorinity and density. We refer to this phenomenon as "volatility", which is broadly associated with substantial increases in the HCl/NaCl ratio (eventually to >1) due to hydrolysis of NaCl. Some transition metals (e.g., Fe, Zn) exhibit volatility prior to halite stability, suggesting a potential shift in vapor speciation relative to nearer critical regions of the vapor–liquid solvus. The chemistry of deep-sea hydrothermal fluids appears affected by this process during magmatic events, however, our results do not support suggestions of subseafloor halite precipitation recorded in currently available field data. Ca–Cl systematics in vent fluids are specifically explored, revealing behavior consistent with partitioning due to phase separation. Interestingly, the effect of variable chloride on dissolved Na/Ca ratios associated with plagioclase solubility (in single-phase solutions) appears fundamentally similar to that of phase separation on vapor compositions such that vapors evolved in hydrothermal systems may naturally remain near equilibrium with the host lithology. Conversely, residual liquids/brines left behind in the crust may be undersaturated with metals, enhancing the rate and extent of hydrothermal alteration.
Published by Elsevier Ltd.

* Corresponding author at: Earth Sciences Division, Lawrence Berkeley National Laboratory, One Cyclotron Road, Berkeley, CA 94720, USA.
E-mail address: NJPester@lbl.gov (N.J. Pester).

http://dx.doi.org/10.1016/j.gca.2015.07.028
0016-7037/Published by Elsevier Ltd.

1. INTRODUCTION

Relative to precursor seawater, the chemistry of deep-sea hydrothermal fluids exhibits variable enrichment in trace alkalis (Li, K, Rb), alkaline earths (Ca, Sr, Ba), transition metals (Mn, Fe, Cu, Zn) and dissolved gases (H_2, H_2S) depending on temperature, fluid/rock ratio, and the lithology of reacting substrate. The most important ligands for aqueous metal transport in natural systems are Cl^-, HS^- and OH^- (e.g., Crerar et al., 1985; Seward and Barnes, 1997). However, a robust database of natural fluid samples demonstrates the acidic/reducing conditions typical of hydrothermal systems essentially leaves only Cl^- to charge balance cations in solution (e.g., Von Damm et al., 1985b; Campbell et al., 1988; Butterfield et al., 1994; Edmond et al., 1995; Douville et al., 2002; Seyfried and Shanks, 2004; Schmidt et al., 2007; Mottl et al., 2011; Reeves et al., 2011; German and Seyfried, 2014). Such studies further reveal the Na/Cl ratios in these fluids are minimally depleted (if at all) relative to the seawater value of 0.85. The physical properties of NaCl solutions are, therefore, commonly accepted as analogous to those of circulating hydrothermal fluids (Bischoff and Rosenbauer, 1984, 1985), which appear to routinely intersect the two-phase boundary resulting in the formation of lower and higher density/chlorinity vapors and liquids, respectively, that can coexist at equilibrium (Bischoff, 1991). This is exemplified by temporal and/or spatial variability in the chloride concentrations of fluid samples acquired from a variety of locales (5–200% of seawater values) and consistent with high chlorine alteration minerals (amphiboles) in dredged rift samples (Ito and Anderson, 1983; Vanko, 1986) and fluid inclusions of variable salinity (from CO_2-rich vapors to 50 wt% Na–Ca–Cl brines with sulfide daughter crystals) in alteration assemblages of both ophiolites and active spreading centers (Kelley and Delaney, 1987; Nehlig, 1991; Saccocia and Gillis, 1995; Vanko and Laverne, 1998; Kelley and Fruh-Green, 2001; Vanko et al., 2004). Furthermore, excess chlorine observed in some fresh MORB glasses suggests assimilation of a concentrated brine or halite near the magma-hydrothermal interface prior to eruption (Michael and Cornell, 1998; Coombs et al., 2004; le Roux et al., 2006). Such data are not only consistent with phase separation, but also phase segregation, wherein the lower density/salinity vapor buoyantly rises to vent at the seafloor and the more saline liquid possibly becomes sequestered in lower permeability regions of the crust (Saccocia and Gillis, 1995; Fontaine and Wilcock, 2006). The preferential partitioning of solutes between liquids and vapors can thus serve to modify the pH, oxidation state and/or electrolyte/volatile contents of the evolving fluids (Drummond and Ohmoto, 1985; Trommsdorff and Skippen, 1986; Bischoff and Rosenbauer, 1987; Giggenbach, 1997; Heinrich et al., 1999; Williams-Jones et al., 2002; Arnorsson et al., 2007; Foustoukos and Seyfried, 2007a).

Partitioning of a solute between equilibrium liquid and vapor phases is often described in terms of a distribution constant such as

$$K_d = M_{vap}/M_{liq} \quad (1)$$

where M_{vap} and M_{liq} are the concentrations of the solute in the coexisting vapor and liquid, respectively. K_d has also been referred to as a "volatility ratio" (Drummond and Ohmoto, 1985) for the intercomparison of solute affinity for the vapor phase. Along the H_2O steam saturation curve, partitioning of non-electrolytes is well characterized by the thermodynamic formulation of Japas and Levelt Sengers (1989); and K_d values are therefore calibrated for many species as a simple function of temperature given the fixed densities of the coexisting vapor and liquid (Fernandez-Prini et al., 2003). For example, the K_d values of H_2S and H_2 (infinite dilution) at 350 °C are approximately 5.1 and 16.1, respectively, illustrating both gases are more soluble in the vapor than the liquid ($K_d > 1$), but the solubility of H_2S in the liquid is higher than that of H_2. Note also that K_d should converge to unity at the H_2O critical temperature (373.9 °C), a relationship obeyed by the non-electrolytes where such data are available (Japas and Levelt Sengers, 1989; Fernandez-Prini et al., 2003).

The application of similar thermodynamic formulations to electrolytes is more tenuous (especially due to their high solubility in the liquid), requiring knowledge of or assumptions regarding activity/speciation in the coexisting aqueous phases (Simonson and Palmer, 1993; Alvarez et al., 1994; Palmer et al., 2004). Furthermore, such equations cannot account for phase behavior in multicomponent solutions at conditions beyond the critical point of pure H_2O. Decades of experimentation, however, have empirically characterized the P–V–T–x (pressure–volume-temperature-salinity/chlorinity) properties of coexisting vapors and liquids in the NaCl–H_2O system (Sourirajan and Kennedy, 1962; Khaibullin and Borisov, 1966; Bodnar et al., 1985; Bischoff et al., 1986; Rosenbauer and Bischoff, 1987; Bischoff and Rosenbauer, 1988; Knight and Bodnar, 1989; Marshall, 1990). These data have been particularly helpful as a means to interpret the physical and chemical conditions reflected in the chemistry of deep-sea hydrothermal fluids and relict alteration minerals. In many instances, predicted temperatures (~400–475 °C) and the associated pressures (~250–500 bars) are well above the critical point of pure H_2O (Gillis, 1995; Foustoukos and Seyfried, 2007b; Fontaine et al., 2009; Alt et al., 2010; Pester et al., 2011, 2012), where a 3D critical curve exists in P–T–x space (e.g., see Fig. 2). We refrain, however, from using the terminology "supercritical phase separation" commonly found in related literature, as this is essentially a chemical misnomer that was adopted in reference to the critical point of water. Furthermore, this terminology is inconsistently applied to mean relative to the critical point of pure H_2O or seawater (407 °C, 298 bars, Bischoff and Rosenbauer, 1988), both of which are arbitrary constraints due to subseafloor phase segregation and open system behavior (Liebscher and Heinrich, 2007).

Vapors in deep-sea hydrothermal systems appear to evolve at P–T conditions near the NaCl–H_2O critical curve (Pester et al., 2014a, 2014b), and can have chloride concentrations approximately two orders of magnitude higher than those at steam saturation ($T < 374$ °C). It is therefore important to better assess the effects of phase separation on pH and metal transport at these conditions, especially given

the relatively low chlorinity and pH of hydrothermal fluids observed in the aftermath of eruptions and other subseafloor magmatic events (Von Damm, 2000; Lilley et al., 2003; Seewald et al., 2003; Seyfried et al., 2003; Pester et al., 2014a). While the overall metal concentration in hydrothermal fluids is controlled to a first order by temperature dependant mineral solubility, phase separation can potentially be decoupled from fluid-mineral equilibria depending on flow rate/residence time considerations. Our experimental investigation is focused primarily on divalent metals, which appear to partition into the liquid phase more than Na and other alkalis (Berndt and Seyfried, 1990; Foustoukos and Seyfried, 2007c). This not only makes it more likely for the effects of phase separation to be resolved in vent fluid data, but also suggests the importance of considering such partitioning in the development of fully coupled multiphase reactive transport models. There are several previous investigations of minor metal partitioning relevant to our current study that have provided important insight into this subject (Bischoff and Rosenbauer, 1987; Berndt and Seyfried, 1990; Simon et al., 2004; Pokrovski et al., 2005,2008; Foustoukos and Seyfried, 2007a; Rempel et al., 2012). However, due to smaller data sets and/or differing experimental conditions, sufficiently accurate partition coefficients have yet to be derived for a range of components particularly important to the evolution of seafloor hydrothermal systems. Herein we report data obtained from multiple hydrothermal flow experiments conducted at temperatures between 360 and 460 °C and pressures coincident with vapor–liquid/vapor-halite stability. Furthermore, this is the first study to explicitly examine the behavior of divalent metals and pH at and near halite saturated conditions.

2. EXPERIMENTAL PROCEDURES

2.1. Flow-through experimental design

Flow experiments were carried out in one of two functionally similar hydrothermal pressure vessels, but constructed of different materials. Exps. 1–3 were conducted in a 316 stainless steel reactor (~110 cm^3), whereas Exps. 4–8 utilized a newly designed Ti-alloy reactor (~165 cm^3). The experimental design is similar to that described in Foustoukos and Seyfried (2007c) with modifications as shown in Fig. 1. Capillary pressure tubing (1/16" O.D.) connected the reactors to all external valves and pumps. For the Ti-alloy cell, all wetted accessory tubing and valves (including the pump head) were also constructed of Ti with exception of the back-pressure regulating valve (316ss). The vapor output line was run through a cold water bath to assure warm fluid was not entering the back-pressure regulator. Reaction vessel temperature was maintained by three independent external heating coils using proportional control microprocessors. The temperature input signal for each controller was provided by thermocouples placed in external wells drilled in the side of each vessel. The reactors were insulated in a 2" thick calcium-silicate cylinder packed with

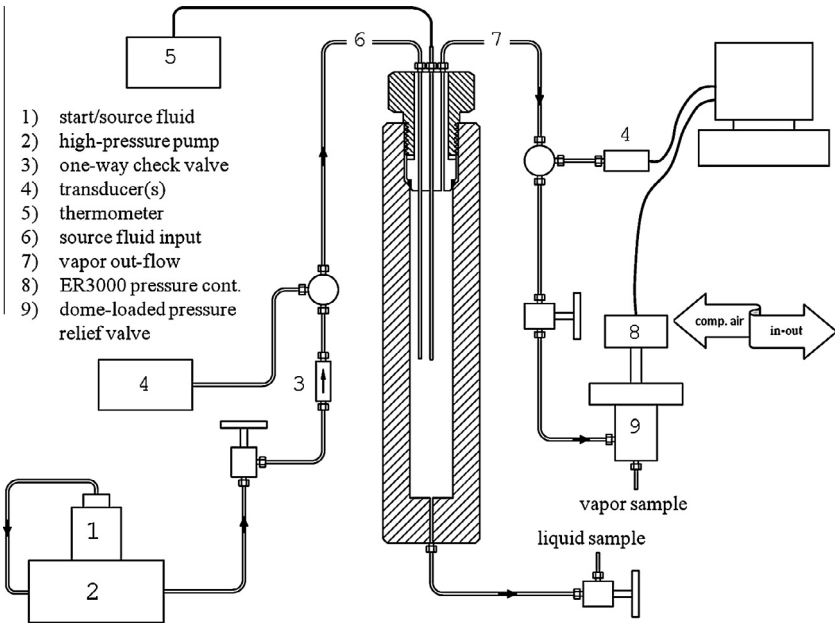

Fig. 1. Schematic diagram of the experimental flow system and Ti-alloy reaction cell used for the present study. Source fluid input line (6) terminates mid-cell as does the internal (Ti-sheathed) thermocouple where temperature is logged by the digital thermometer (5). The centered location of the input line terminus helps to maximize residence time for vapor–liquid segregation (i.e. farthest from the vapor and liquid sampling ports). External thermocouples and heating coils related to cell temperature control are not shown for clarity (see text for description). Static pressure is maintained via computer interface between a transducer (4.2) and the ER3000™ unit (8) containing solenoid valves that rapidly inlet/exhaust compressed air to the dome of the pressure relief valve (9). Liquid samples were periodically retrieved using a manual valve. See text for details.

glass wool. Thermocouples were also used to directly monitor the internal fluid phase(s) where the temperature was typically 3–7 °C higher than the external set-point from 400 to 500 °C, respectively. Given internal T was monitored near the terminus of the input capillary, this demonstrates incoming fluid was sufficiently pre-heated to avoid any cold fingering effects. Thermocouples were calibrated against the steam saturation pressure of pure H_2O up to 360 °C and those used for internal solution monitoring were further calibrated up to 500 °C using a P–T isochore ($\rho = 0.45$ g/cm^3) for a known mass of pure H_2O in the fixed volume cell. Steel-sheathed (1/16") mineral-insulated thermocouples (Type J, iron-constantan) were used with the exception that a Ti-sheathed Type E (chromel-constantan) thermocouple was used for internal monitoring of the Ti-alloy cell. Temperatures reported herein refer to those measured in direct contact with the internal fluid phase. Average, minimum and maximum interior temperatures were monitored for each set-point. The min/max deviation from the average value was typically ±1–2 °C but was, in a few cases, as high as 4 °C at conditions associated with halite stability. The latter is thus the most conservative temperature error, which is greater than the reported uncertainty of the thermocouples. External temperatures remained invariant from the set (control) temperature. Pressure was logged for each set-point using two in-line pressure transducers, one of which provided the input signal to the back-pressure regulator. Uncertainties in pressure are constrained by the capability of this regulator (±0.5 bars under experimental conditions), which is an air actuated (dome-loaded) valve connected to an ER3000™ electronic pressure controller (Tescom Industrial Controls, see Fig. 1). Valve response time is ~0.5 s for the full pressure range, allowing decreases in pressure to be exacted without initially undershooting the set-point.

Vapor samples were collected after having passed through the back-pressure regulator to avoid any unnecessary decreases in pressure associated with opening a discrete sampling valve to the pressurized exit line. This is important due to the P–T sensitivity of vapor chlorinity at near-critical conditions. Though operating at ambient temperature, there was still concern of metal contamination for the most dilute and acidic vapors due to contact with 316ss in the valve. However, a test using 0.05 N HCl (trace-metal grade) for similarly short residence times showed nmolal (negligible) quantities of Fe and Ni. In Exps. 6–8, a computer controlled Ti metering valve was utilized to eliminate any possible contamination; and in these cases pressure variability was ±2–3 bars. Liquid samples were taken, after a sufficient amount of vapor had been acquired, by opening a manual, flow-regulating valve (Ti). With one exception (6-L4), liquid samples were not acquired in Exps. 6–8 due to the more sluggish response of the Ti metering valve.

All starting solutions were prepared with deionized H_2O and ACS grade chloride/bromide salts with the exception that Ni (Exp. 6) was introduced by dissolving the native metal in HCl. In some experiments the bulk concentrations of Fe and Ca were elevated in a manner consistent with that of natural hydrothermal fluids (10 and 20 mmolal, respectively). All solutions were titrated to a pH of ~3.0 with HCl prior to the addition of variably small amounts of formic acid. Upon heating, formic acid breaks down into equimolar amounts of CO_2 and H_2 and was thus used to assure the fH_2 in the cell was more than adequate to maintain redox sensitive transition metals in the most reduced state. This also precluded precipitation of Fe-oxides given the low pH in the system. Measured H_2 concentrations in the single/vapor phases ranged 2.5–16 mmol/kg. Dissolved gas concentrations (CO_2, H_2, CH_4, CO) are reported from Exps. 2–4 (Tables S.2–S.4) when monitored for reproducibility.

Throughout the experiments (and for 24 h prior), starting solutions were continuously purged with either N_2 or CO_2 directly in the reservoir for the delivery pump to remove dissolved oxygen. Prior to introduction of a given source fluid, the reactor (at ambient conditions) was also flushed with N_2. The pre-purged starting solution was then introduced into the bottom of the cell (liquid-sampling line, Fig. 1) until the internal volume of N_2 was fully displaced (out the vapor-sampling line). At this point the liquid sampling valve was closed and the cell was heated, using the back-pressure regulator to maintain pressure (while evacuating excess fluid) equivalent to ~15–20 bars above the associated critical pressure for the target temperature, given also the bulk salinity of the starting solution. Eventually, flow of the starting solution was resumed, now being pumped in through tubing that terminated near the center of the internal cavity (Fig. 1). High-temperature, single-phase flow was maintained until steady-state pH (25 °C) and dissolved gas concentrations (CO_2, H_2) were achieved. At this point a fluid sample was acquired (denoted S in Supplementary Data Tables). The chemical composition of this sample was compared to the reservoir solution to assure the effect of dissolution/precipitation reactions occurring in the cell was negligible. For most elements/experiments, the %RSD (2σ) between the start solution and the reacted (single-phase) solution was always less than 4%, but in the case of Exp. 4, Fe and Cu in the latter were elevated by 6% and 11%, respectively. Greater variability was noted for Fe and Cu in Exp. 8, although the cause of this is unclear. The chemistry of both the reacted fluid and the starting fluid are therefore given in Table S.8.

While flowing continuously, the two-phase region was typically approached by decreasing the set pressure on the back-pressure regulator along a given isotherm. Increasing temperature at constant pressure was also employed, especially as a means to approach the halite stability field at pressures consistent with seafloor constraints ($P >$ ~200 bars). At conditions in the two-phase region, flow rate of the source fluid was typically 0.1–0.3 g/min, sufficient to give steady-state vapor chlorinity in good agreement with those predicted for equilibrium in the NaCl–H_2O system (Fig. 2). This confirms the concentration range of minor species studied did not appreciably affect phase relations. When a new P–T set-point was imposed, the RI (refractive index, NaCl), pH (25 °C) and dissolved gas concentrations were monitored until the new steady-state vapor composition was established. Usually only 15–20 min was required to achieve steady state, however, fluid was allowed to flow for at least 45 min prior to

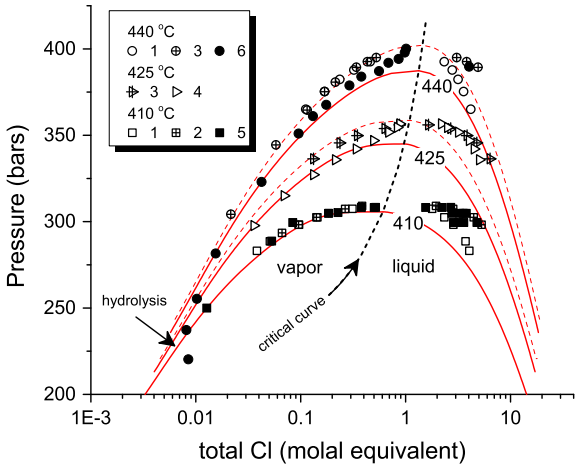

Fig. 2. Isothermal representation of vapor–liquid phase relations for a portion of the NaCl–H_2O system (Driesner and Heinrich, 2007) compared with experimental data presented herein (Tables S.1–S.6), including those of Berndt and Seyfried (1990). Isotherms for temperatures emphasized in this study (410, 425 and 440 °C) are shown (solid lines) in addition to 430 and 445 °C for reference (dashed lines). The critical curve (dashed, shown from 390 to 450 °C) separates the vapor and liquid limbs of the two-phase envelope. Experimental concentrations are total dissolved Cl comparable to the NaCl (molal) equivalent represented in the model isotherms. Low *P* vapor data from Exp. 6 exemplify effects of hydrolysis (Eq. (2)) at/near halite saturation (see Fig. 3).

acquiring samples for chemical analysis. A summary of experimental conditions and starting solution compositions is presented in Table 1.

2.2. Analytical procedures

Samples were collected in either sterile plastic syringes (with PTFE stopcocks for gas analyses) or pre-weighed, acid-cleaned LDPE bottles for immediate dilution with either a trace-metal grade HCl (for metal analyses) or deionized water (for Cl, Br analyses). The amount of sample acquired and the associated dilution factors were scaled based on the RI (or predicted phase compositions for vapors below detection by RI) such that accurate analysis of the minor metals could easily be achieved. For example, large samples of the highly dilute vapors (~10–20 ml) were taken, which is a distinct advantage of the flow-through configuration. Two hand-held refractometers were used in the course of the experiments for monitoring chlorinity changes, both factory calibrated to reference concentration in wt% NaCl. One spanning the range 0–26 wt% was used for the liquids whereas another, having a more refined range of 0–10 wt%, was used for the vapors.

Cl and Br were analyzed by ion chromatography (2σ: ±1% and 3%, respectively) and all cations were analyzed by inductively-coupled plasma optical emission spectroscopy (ICP-OES) with uncertainties of ±4% (2σ). The vapors of Exps. 7–8 (363 °C) were extremely dilute and were therefore analyzed by inductively-coupled plasma mass spectrometry (ICP-MS). For most metals the uncertainty in these analyses is ±5% (2σ). The reproducibility

Table 1
Summary of experimental conditions and source fluid compositions.

Exp 1–0.62 molal NaCl, 0.87 mmolal NaBr		
V(5) + L(5)[a]	410 °C	307–283 bars
V(5) + L(5)	440 °C	393–365 bars
V(4) + L(3)	447–482 °C	400 bars
Exp 2–0.57 molal NaCl, 11 mmolal $FeCl_2$, 1 mmolal $MnCl_2$		
V(6) + L(5)	410 °C	309–294 bars
Exp 3–0.95 molal NaCl, 11 mmolal $FeCl_2$, 1 mmolal $MnCl_2$		
V(5) + L(5)	425 °C	356–336 bars
V(7) + L(3)	440 °C	395–344 bars
V(1) ± L-H	440 °C	304 bars
Exp 4–0.93 molal NaCl, 2 mmolal $CaCl_2$, CuCl, $FeCl_2$, $MnCl_2$, $SrCl_2$, $ZnCl_2$		
V(9) + L(6)	425 °C	357–298 bars
V(3) ± L-H	465 °C	298–247 bars
Exp 5–0.61 molal NaCl, 20 mmolal $CaCl_2$, 2 mmolal $MnCl_2$, $SrCl_2$, $ZnCl_2$		
V (7) + L(11)	410 °C	308–250 bars
V(3) ± L-H	410–453 °C	250 bars
Exp 6–0.99 molal NaCl, 1 mmolal $CaCl_2$, CuCl, $FeCl_2$, $MnCl_2$, $SrCl_2$, $ZnCl_2$, $BaCl_2$, $CoCl_2$, $NiCl_2$, $MgCl_2$		
V(11) + L(1)	440 °C	398–323 bars
V(4) ± L-H	440 °C	282–220 bars
Exp 7–0.2 mmolal NaCl, 250 μmolal $CaCl_2$, $SrCl_2$, $BaCl_2$, $MgCl_2$		
V(13) + L(0)	363 °C	189–150 bars
V(2) ± L-H	363 °C	104–70 bars
Exp 8–0.2 mmolal NaCl, 250 μmolal $CaCl_2$, CuCl, $FeCl_2$, $MnCl_2$, $SrCl_2$, $ZnCl_2$, $BaCl_2$, $CoCl_2$, $MgCl_2$		
V(6) + L(0)	363 °C	185–125 bars
V(3) ± L-H	363 °C	112–65 bars

[a] Number of vapor (V) or liquid (L) samples acquired.

for Mg and Ca was considerably worse; but these data are still reported unless the error exceeds 25%. Dissolved gas concentrations were analyzed after head-space extraction using a gas chromatograph equipped with both a thermal conductivity detector and a flame ionization detector (including a methanizer). Target species were separated using a carboxen 1010 plot column. pH (25 °C) was measured using a Thermo-Ross electrode that was continuously calibrated throughout each experimental session. We note that no effort has been made to correct for the effect of high salinity on the liquid junction potential of the electrode, which may be a minor source of error for some of the liquid phase samples (Knauss et al., 1990). pH was measured on multiple discrete samples immediately after retrieval to avoid metal oxidation and attending acidification, which especially affected the liquid samples as suggested by decreasing pH measured on the same sample with increasing time. For example, some of the heavier brines (unpreserved) showed visible precipitate and pH values lower than the vapor counterpart after less than 24 h.

The full fluid chemistry of Exps. 1–8 are given in Tables S.1–S.8 (Supplementary Materials). For most samples of Exps. 2–8, chloride is calculated based on charge balance of the suite of cations in solution. This includes HCl via pH measurement, which is an important constraint for the more dilute vapors (see Section 3.3.1). Chloride was independently analyzed for several samples to verify agreement with the calculated values (Table S.9).

3. RESULTS

3.1. Agreement with predicted NaCl–H_2O (vapor–liquid) phase equilibria

Vapor-phase chlorinity was generally reproducible for equivalent *P*–*T* conditions. However, there were changes in the internal fluid temperature with decreasing pressure in the two-phase region despite consistent external temperature control. This results, for example, in the difference in chlorinity trends between Exp. 3 (425 °C), where *T* remained constant, and Exp. 4 (425 °C), where the *T* dropped over 6 °C attending decompression (Table S.4, Fig. 2). For most experiments, we did not correct for this by changing the external set-point. Such decreases in *T* are consistent with continuous effects of latent heat given the open (flowing) nature of the experimental design. In general, our vapor data agree with model (NaCl–H_2O) isotherms ~2–5 °C higher than the actual measured temperatures. This is nonetheless excellent agreement given current models of vapor–liquid equilibria are empirical fits of data acquired using a variety of experimental methods (Bischoff and Pitzer, 1989; Driesner and Heinrich, 2007). We do note that several thermodynamic equations of state have been developed for the NaCl–H_2O system (Hovey et al., 1990; Anderko and Pitzer, 1993; Pitzer and Jiang, 1996; Oscarson et al., 2004; Sedlbauer and Wood, 2004; Liu et al., 2006), but these too rely heavily on the same experimental data.

The disadvantage of the flow-through configuration is manifest by acquisition of liquid-phase samples with higher chlorinity than predicted for equilibrium (Fig. 2). It has long been recognized that agitation by either stirring or rocking of experimental cells is beneficial for obtaining the equilibrium liquid phase (Khaibullin and Borisov, 1965; Bischoff and Rosenbauer, 1987; Berndt and Seyfried, 1990; Shmulovich et al., 1999). Unlike the vapor phase that must be salt-saturated, brine condensation can result in metastable density stratification. An exercise conducted during Exp. 5 demonstrates the existence of stratification in the liquid phase (Fig. S.3). Predicted liquid equilibrium thus proved unattainable with the open system configuration of these experiments, especially given our inability to sample liquids more closely associated with the (mobile) vapor–liquid interface. This explains the irreproducibility of the liquid phase chlorinity despite consistency for the vapor phase. We will demonstrate, however, that the majority of quantifiable fractionation of minor metals is expressed in the vapor.

3.2. pH and reaction cell composition

There is a clear difference in the vapor Cl vs. pH trends of the experiments carried out in the 316ss cell relative to those in the Ti-alloy cell. While the Ti cell (expectedly) exhibits little reactivity, it appears the 316ss cell modifies the pH to values higher than those of the starting solutions for the single-phase fluid and vapors of intermediate chlorinity

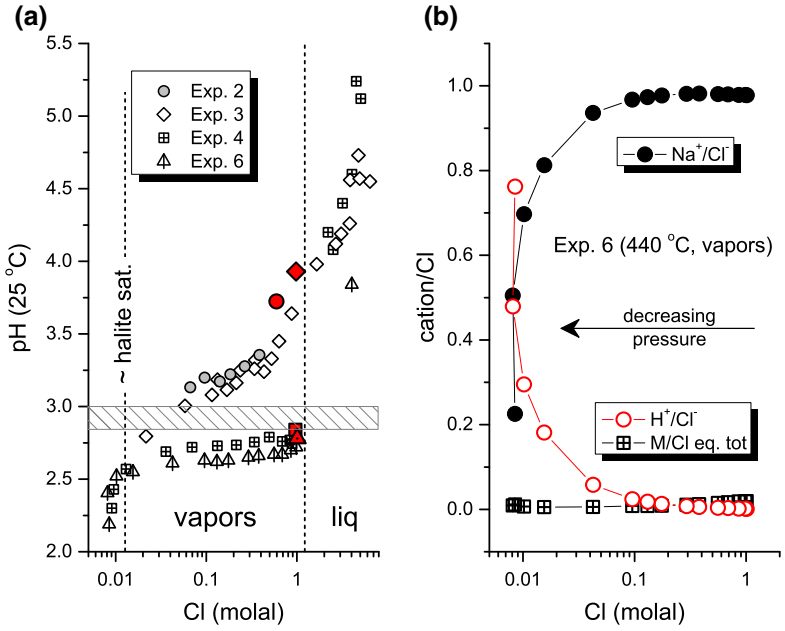

Fig. 3. (a) Experimental pH (25 °C) vs. Cl. Hatched area (pH ~ 2.8–3.0) represents pH values of starting solutions prior to having passed through the reactor at high temperature. For individual experiments, larger filled symbols of corresponding shape are the reacted single-phase fluids. Exps. 2 and 3 were carried out in the 316ss flow cell whereas Exps. 4 and 6 were carried out in the Ti alloy cell. The 316ss appears to modify the pH of the single/vapor phase fluids to values higher than the incoming source fluid, though these effects decrease with vapor chlorinity. pH was always higher in the liquid samples, further demonstrating the high vapor affinity of HCl. Abrupt decreases in pH were observed at/near halite saturation (b) H^+/Cl^- ratio compared to that of Na^+/Cl^- (context of total cation charge balance) in vapors attending decompression in Exp. 6. In-situ HCl generation due to NaCl hydrolysis (Eq. (2)) accounts for the concomitant decrease and increase in Na^+/Cl^- and H^+/Cl^-, respectively.

(Fig. 3a). In these cases (Exps. 2 and 3), the observed decrease in pH (25 °C) with chlorinity/density results from a combination of the decreasing residence time of the vapor (i.e. time to react with the cell) as well as decreasing activity of H^+ due to the increasing association constant (K_a) of HCl (Ho et al., 2001). In addition to pH changes, reactivity of the 316ss cell should be expected to contribute, for example, excess Fe. As illustrated below, however, this did not pose a problem in these experiments (2 and 3) due to the relatively high Fe (and Mn) concentrations in the source fluid (Table 1).

3.3. Partitioning of alkaline earth and transition metals

Given charge balance must be conserved, the vapor–liquid partitioning of metals in a chloride matrix is most simply demonstrated by a change in the metal/chloride ratio (M/Cl, molal) relative to that of the precursor (single-phase) starting solution. Within the two-phase region, evolved (higher chlorinity) liquids retain M/Cl ratios consistent with those of the starting solution, due mostly to mass balance constraints. Conversely, quantitative changes take place in the vapor composition as chlorinity and density decrease with increasing extent of phase separation (Fig. 4). Thus, for the systems studied here, vapor–liquid partitioning of minor metals within the broader NaCl–H_2O system appears predictable over a broad range of the two-phase envelope in a manner that is independent of P and T. Prior to full treatment of these data, however, we first note divergent behavior in vapor chemistry observed at/near halite saturation.

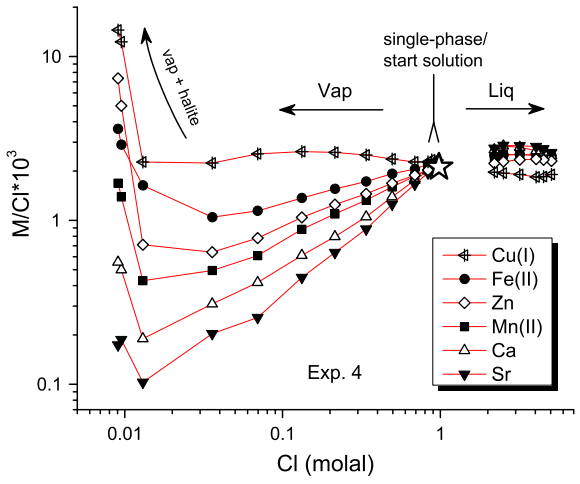

Fig. 4. Metal/Cl (M/Cl) ratio vs. Cl in Exp. 4. The M/Cl was roughly equivalent for all minor metals in the single-phase/start solution (star). Coexisting vapor and liquid chlorinity decreases and increases, respectively, with the extent of phase separation. Accordingly, divalent metals exhibit quantifiable decreases in vapor affinity until halite saturation is approached and apparent "volatility" (Section 3.3.1) is observed. The two lowest chlorinity samples represent vapor-halite coexistence. Due to mass balance, there is little change in the M/Cl with increasing liquid chlorinity, though the values are slightly offset relative to the start solution in a manner inverse with observed trends in the vapor.

3.3.1. Metal volatility and hydrolysis at extreme P–T conditions

At sufficiently extreme two-phase conditions (relatively low isothermal P and/or high isobaric T) the liquid becomes (halite) saturated, and chloride-normalized metal concentrations increase abruptly in the vapor phase (Figs. 4, S.5, Cl < ~0.01 molal). This behavior is similar to the observations of Foustoukos and Seyfried (2007c) for trace alkalis (Li, Rb, Cs) and Br. For the divalent metals, however, this constitutes an unexpected reversal in the trends of decreasing vapor affinity with chlorinity/density along most of the vapor branch; and herein we refer to this phenomenon as "volatility". Data of both Exps. 4 and 6 further demonstrate Cu(I), Fe(II) and Zn(II) able to increase in concentration and achieve M/Cl ratios in excess of the starting fluid (Figs. 4, S.5). This volatility is often associated with a sharp decrease in the Na/Cl ratio and pH (25 °C), indicating halite hydrolysis (Figs. 2, 3) (Armellini and Tester, 1993; Fournier and Thompson, 1993; Liebscher, 2007) as follows:

$$NaCl_{(S)} + H_2O_{(V)} = NaOH_{(S)} + HCl^0_{(V)} \quad (2)$$

Though K_d values for HCl highly favor concentration in the vapor (Simonson and Palmer, 1993), source fluid compositions (pH) were not sufficient for partitioning to account for the low pH (25 °C) of halite saturated vapors; and mass balance requires in-situ acid generation (via Eq. (2)) in order for HCl to surpass NaCl as the dominant vapor species. For example, Fig. 3b reveals a nearly 1:1 correspondence between increases and decreases in H^+/Cl^- (or hydronium/Cl) and Na^+/Cl^- ratios respectively. These data further support the suggestion that vapor-halite coexistence is required for significant hydrolysis in NaCl dominated systems (Fournier and Thompson, 1993), contrasting with the system $CaCl_2$–H_2O wherein HCl is abundantly produced on the vapor–liquid solvus (Bischoff et al., 1996). The Ca (and other metal) concentrations in our experiments, however, are sufficiently low that possible contributions to the hydrolysis effect are not clearly resolved in the data. Furthermore, the increase in vapor M/Cl with halite stability for all the minor metals suggests their incorporation in solid hydroxide or oxide phases with lower solubility than Cl-bearing salts (similar to Eq. (2)) is not as significant as it is for Na, although, hydrolysis of the alkaline earths may be occurring at the most extreme conditions (see Fig. S.5). An implicit connection between saturation ± hydrolysis and metal volatility, however, is not clear. It is broadly counterintuitive that equilibrium precipitation of any saturated solids/minerals might enhance the solubility of the constitutive metals in the coexisting aqueous phase(s). Volatility may reflect preferential exclusion from the halite lattice (Foustoukos and Seyfried, 2007c), a simple explanation given our observations expand the occurrence of this phenomenon to a more diverse suite of cations. Still, we can place little further constraint on the nature of solids that may be coexisting with vapor ± liquid at these extreme conditions, or their influence on volatility, especially considering potential complications such as precipitation kinetics or, for example, the low melting temperature of a likely candidate such as Na_2ZnCl_4 (410 °C, Rice and Gregory, 1968).

3.3.2. Normalization of vapor data and partitioning behavior of minor metals

Barring conditions approaching halite stability, there is a broad region of vapor–liquid coexistence where, for each minor element, the change in M/Cl with chlorinity in the vapor gives a nearly equivalent slope regardless of the M/Cl of the single-phase/start solution (Fig. 5). This slope may be defined as S_V for the vapor limb. Given the consistency of S_V despite variable P–T conditions (and an order of magnitude M/Cl, Fig. 5a), we can normalize the vapor compositions from different experiments to that of the associated starting fluids (Fig. 6) and regress a partition constant defined as $B_{V/S}$ where

$$\log(M_{\text{vap}}/M_{\text{start}}) = B_{V/S} * \log(\text{Cl}_{\text{vap}}/\text{Cl}_{\text{start}}) \quad (3)$$

and M_{vap}, Cl_{vap} and M_{start}, Cl_{start} are the metal and Cl concentrations in the vapor and starting solutions, respectively. This relationship requires that regression of the vapor data pass through the graphical origin; and the slope ($B_{V/S}$) for each minor metal is inherently normalized to Na ($B_{V/S} \approx 1$), which ultimately dictates phase behavior in both the experiments and marine hydrothermal systems (Fig. 6). Similar to our work, minerals were not present in the experiment of Berndt and Seyfried (1990), and these data are included in the regressions. The data of Exps. 7–8 (~360 °C) were not included in any regressions for reasons discussed later

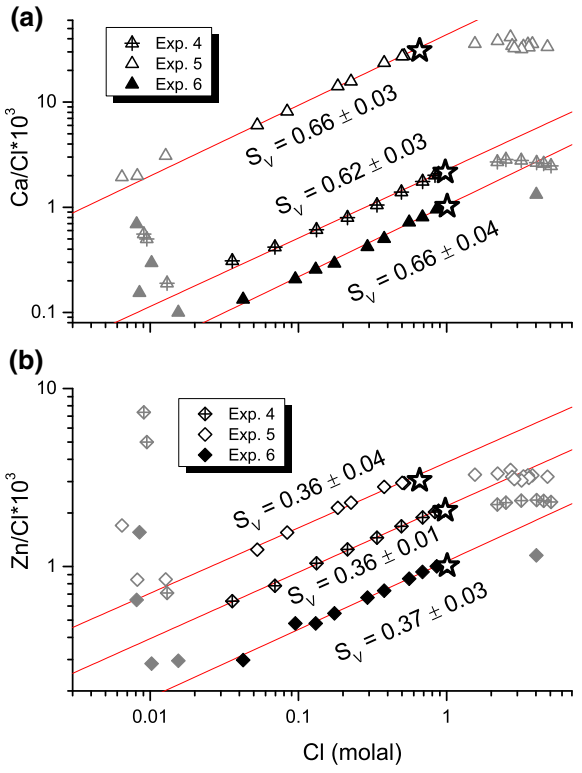

Fig. 5. Cl vs. (a) Ca/Cl, and (b) Zn/Cl for Exps. 4, 5 and 6. The slope of regressions (S_V) for the non-volatile vapor samples (see text) are nearly equivalent regardless of the M/Cl of the single-phase fluid (stars). Corresponding liquid-phase samples and volatile vapor samples not included in the regressions (see Fig. 6) are shown in grey-scale.

(Section 4.1). $B_{V/S}$ values are given in Table 2. As a result of this normalization, S_V (Fig. 5) can also be more accurately defined as:

$$S_V = B_{V/S} - 1 \quad (4)$$

In application to natural hydrothermal systems, these relationships simplify modeling certain aspects of phase separation given assumptions regarding the composition of subsurface liquids will often be required. Though not incorporated in $B_{V/S}$ regressions, the similarly normalized liquid compositions, again, show little deviation or change in slope (Fig. 6). However, for metals with $B_{V/S} > 1$, a slight parallel offset above the unity line is observed that generally increases with $B_{V/S}$ and the Cu(I) data fall below unity in a similar manner (see also Fig. 4). Our results for Br (Table 2, Fig. S.4) agree with the majority of previous investigations in that NaBr has a slightly higher vapor affinity than NaCl (Berndt and Seyfried, 1990, 1997; Liebscher et al., 2006; Foustoukos and Seyfried, 2007c).

3.3.3. Vapor–liquid partition coefficients for minor metals

Ideally, a vapor–liquid coefficient is required to describe the bulk system and fully account for mass balance. This can be derived by treatment of the data in the form of

$$\log(M_{\text{vap}}/M_{\text{liq}}) = B * \log(\text{Cl}_{\text{vap}}/\text{Cl}_{\text{liq}}) \quad (5)$$

that can be simplified to

$$\log K_{d(M)} = B * \log K_{d(\text{Cl})} \quad (6)$$

where M_{liq} and Cl_{liq} are the metal and Cl concentrations in the liquid phase, respectively (K_d notation also shown in Eq. (1)). This is similar to the relationship of Eq. (3), allowing a regression through the graphical origin, and the resulting slope (B) characterizes the vapor–liquid partition coefficient (Fig. 7a, again, $B \approx 1$ for Na). However, in this case, the origin (where $K_d = 1$) strictly represents a position along the system's critical curve, whereas that in Fig. 6 (after Eq. (3)) may represent any position on the two-phase (vapor–liquid) envelope. Fewer data may be treated according to Eq. (6) due to the limited P–T–x range in which liquid samples remain undersaturated in transition to ambient conditions. The data correlations for the B regressions are less robust than those resulting in the $B_{V/S}$ coefficients, likely related to the putative salinity stratification in the liquid phase during the experiments. As might be expected, there is, regardless, a good linear correlation between the $B_{V/S}$ and B values (Table 2, Fig. S.2). This can be used to calculate B with reasonable uncertainty for the divalent metals lacking sufficient liquid phase data for direct regression (e.g., Ni, Co).

The "ray-diagram" approach to solute partitioning (Palmer et al., 2004; Liebscher, 2007; Pokrovski et al., 2013) relates $K_{d(M)}$ to the densities of the coexisting vapor and liquid phases (ρ_{vap} and ρ_{liq}, respectively) as follows:

$$\log \text{K}_{\text{d}(M)} = n * \log(\rho_{\text{vap}}/\rho_{\text{liq}}) \quad (7)$$

rather than the charge-balance approach represented by Eqs. (5) and (6). Noted earlier, the thermodynamic formulation of Japas and Levelt Sengers (1989) has shown such a relationship is valid at the infinite dilution limit (i.e. ρ_{vap}

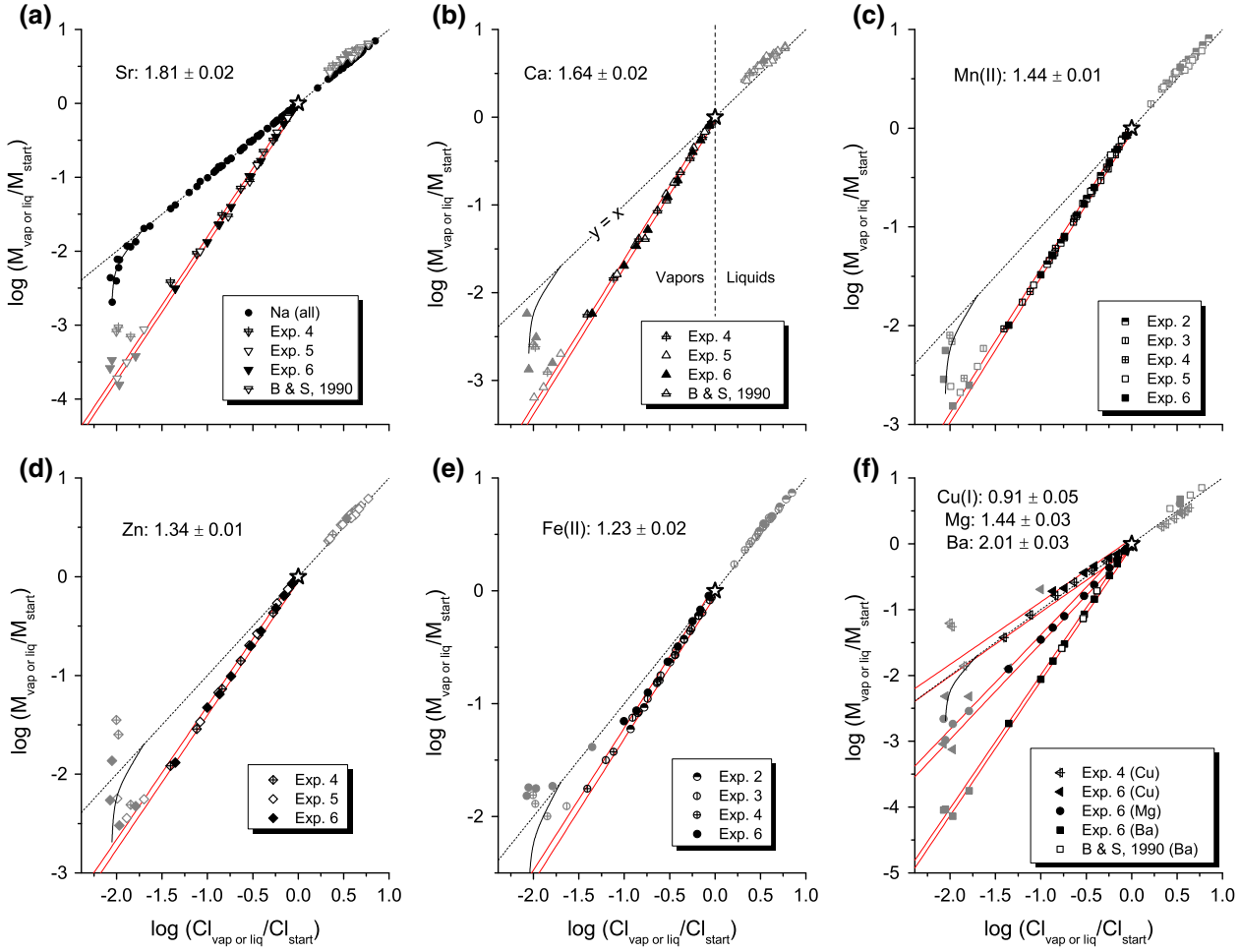

Fig. 6. Experimental data normalized for extraction of vapor-based partition coefficients ($B_{V/S}$, Section 3.3.2) for (a) Sr, (b) Ca, (c) Mn(II), (d) Zn, (e) Fe(II) and (f) Cu(I), Mg and Ba. Panel (a) shows the corresponding Na data from all the experiments. Na expectedly shows no deviation from the unity line (short dash, $y = x$) except at/near halite saturation, likely due to hydrolysis (see text, Fig. 3). A curve fit to this deviation is shown for reference in the other panels. Vapor data are regressed through the origin and the slope constitutes the partition coefficient $B_{V/S}$. Regressions are represented by the 95% prediction limit for each metal and the reported error of $B_{V/S}$ is the 95% confidence interval. Regressions of Ni and Co not shown for clarity. All coefficients are summarized in Table 2. Liquid-phase data ($x > 0$) and "volatile" vapor data not included in the regressions are shown in grey scale. Vapors were considered "volatile" at/near halite-saturated conditions where Na starts to deviate from the unity line ($\sim x < -1.5$). Sample 6-V11 (Exp. 6) was also excluded for Fe and Cu. A similar plot for Br, including additional experimental data from Berndt and Seyfried (1990, 1997); Liebscher et al. (2006) and Foustoukos and Seyfried (2007c) is presented in Supplementary Materials (Fig. S.4).

and ρ_{liq} are that of pure H_2O at steam saturation) to temperatures very near the H_2O critical point for a wide range of non-electrolytes (e.g., Fernandez-Prini et al., 2003); and reasonable agreement with such a formalism has also been suggested for NaCl (Fernandez-Prini et al., 1993; Alvarez et al., 1994). While far from infinite dilution, the NaCl dominated composition of crustal fluids/seawater is the reason why P–V–T–x properties of the NaCl–H_2O system are empirically determined. Models thus readily allow calculation of solution densities in this two component system (Bischoff, 1991; Driesner, 2007), resulting in translation of the ray-diagram concept such that the NaCl solution is the solvent, and partitioning of additional, dilute (relative to NaCl) solutes may be resolved (Pokrovski et al., 2005). In this case density calculations must assume the molality of total chloride is effectively equivalent to mNaCl. This is reasonable for these experiments, even where the vapor HCl/NaCl ratio is high (e.g., Fig. 3b) because at such conditions total Cl is sufficiently low that density is no longer meaningfully different from that of pure water (at equivalent P–T). Empirical density correlations may be used in a manner exclusive of predicted vapor–liquid phase relations (Driesner, 2007; Driesner and Heinrich, 2007), allowing estimation of vapor and liquid densities using explicitly our experimentally measured P–T–x values (Tables S.1–S.8, calculated after Driesner (2007)). This embraces any disagreement with phase equilibria models (i.e. Fig. 2), which is unavoidable. The derivation of partition coefficients according to Eq. (7) inherently implies a linear relationship between log (ρ_{vap}/ρ_{liq}) and log K_d for total chloride ($K_{d(Cl)}$ or $K_{d(NaCl)}$) within the NaCl–H_2O system itself. Accordingly, despite the apparent excess chlorinity

Table 2
Partition coefficients and 95% confidence intervals.

	Samples[a]	$B_{V/S}$[b]	Samples	B[c]	n[d]
Br	18	0.92 ± 0.04	17	0.95 ± 0.01	3.38 ± 0.06
Na	50	1.000 ± 0.003	36	0.991 ± 0.003	3.54 ± 0.03
Cu(I)	18	0.91 ± 0.05	6	0.89 ± 0.02	3.17 ± 0.09
Fe(II)	37	1.23 ± 0.02	19	1.14 ± 0.01	4.07 ± 0.05
Zn	27	1.34 ± 0.01	17	1.17 ± 0.01	4.17 ± 0.08
Ni(II)	10	1.44 ± 0.05		1.23 ± 0.1	4.4 ± 0.4
Mn(II)	46	1.44 ± 0.01	30	1.23 ± 0.01	4.40 ± 0.07
Co(II)	10	1.51 ± 0.04		1.27 ± 0.1	4.5 ± 0.4
Mg	10	1.44 ± 0.03		1.23 ± 0.09	4.4 ± 0.3
Ca	31	1.64 ± 0.02	21	1.35 ± 0.02	4.82 ± 0.1
Sr	31	1.81 ± 0.02	21	1.44 ± 0.02	5.15 ± 0.1
Ba	14	2.01 ± 0.03	4	1.54 ± 0.02	5.51 ± 0.1

[a] Used in regression, including data of Berndt and Seyfried (1990) for Br, Na, Ca, Sr, Ba.
[b] See Eq. (3).
[c] See Eq. (6), Ni, Co and Mg calculated using $B = 0.55*B_{V/S} + 0.44$ (Fig. S.2).
[d] See Eq. (7).

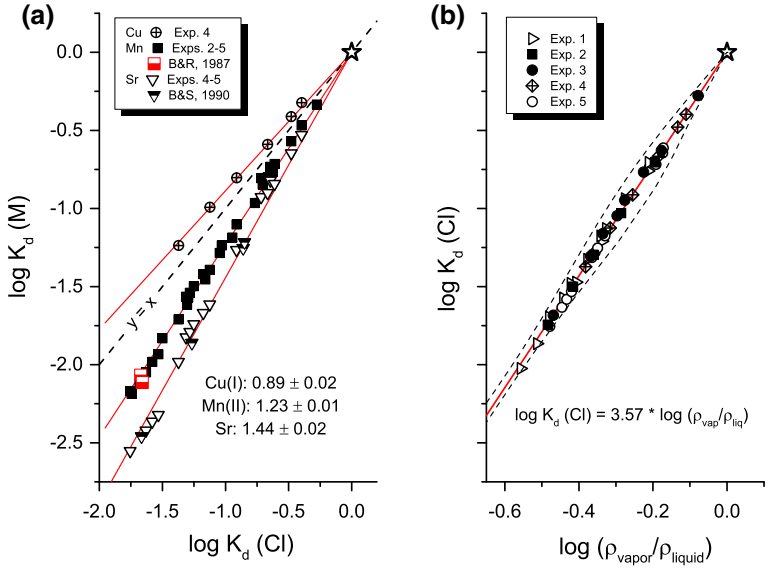

Fig. 7. (a) $\log K_{d(M)}$ vs. $\log K_{d(Cl)}$ for Cu(I), Mn(II) and Sr and regression of the vapor–liquid partition coefficient, B, based on Cl charge balance (see Eqs. (1), (5), (6)), where star symbol is the origin (and critical point). Reported error of B is the 95% confidence interval. Data from Berndt and Seyfried (1990) are included in the Sr regression. Mn data from the two-phase basalt alteration study of Bischoff and Rosenbauer (1987) also show good agreement. B values for all metals are reported in Table 2. (b) The "ray diagram" approach to solute partitioning based on calculated vapor/liquid densities in the NaCl–H_2O system (Eq. (7)). Shown are all vapor–liquid pairs from Exps. 1–5. Vapor/liquid densities (given for all samples in Tables S.1–S.8) were calculated after Driesner (2007) using the experimental P–T–x values. The correlation: $\log K_{d(Cl)} = 3.57 \pm 0.02*\log(\rho_{vap}/\rho_{liq})$, and the resulting relationship $n = 3.57 \pm 0.02*B$ was used to calculate the n values (Eq. (7)) reported in Table 2. The upper and lower (dashed) lines bounding the regression represent independently calculated model isotherms for 600 and 380 °C, respectively (Driesner, 2007; Driesner and Heinrich, 2007). Nonlinearity in these isotherms ultimately reflect uncertainties in empirical representation of near-critical behavior (may or may not be real).

in many of the sampled liquids, an excellent density correlation with $K_{d(Cl)}$ is observed for our reported vapor–liquid pairs that falls within a broader range of independently modeled phase equilibria (isotherms between 380 and 600 °C, Fig. 7b). Therefore, to be internally consistent, n values for minor metals (Eq. (7), Table 2) were calculated after the regression shown in Fig. 7b, and the resulting relationship $n = 3.57 \pm 0.02*B$.

4. DISCUSSION

4.1. Uncertainties and potential limitations

The uncertainties reported for all coefficients ($B_{V/S}$, B, n, Table 2) reflect the 95% confidence interval of regressions (with propagation where appropriate); and the relative differences in partitioning for most metals are statistically

significant. Regardless of general P–T–x conditions, however, the regressions themselves are a necessary oversimplification, being unable to account for likely non-linear behavior at conditions very near the critical curve. Absolute uncertainties are therefore more difficult to constrain. Potential error in B values resulting from the apparent excess salinity of liquid samples may be more easily evaluated by incorporating a limited form of Eq. (3) into a system of mass balance equations (e.g., Berndt et al., 1996; Foustoukos and Seyfried, 2007c) that impose model NaCl–H_2O vapor–liquid phase relations (see Supplementary Materials). These calculations reveal higher B values with maxima on the order of +2% for Fe(II) and increasing to +8% for Ba (Figs. S.1, S.2). While noteworthy, this approach too carries uncertainty, as much closer agreement was observed depending on the NaCl–H_2O equation of state. For general purposes, we therefore see no reason to value these results rather than those obtained by direct regression of the experimental data.

Noted earlier, the P–T conditions explored here are particularly relevant to deep-sea hydrothermal systems, but the empirical construct with which the coefficients were derived (e.g., Fig. 7) indicates they may be relevant over a broader range of P–T space, at least, where NaCl–H_2O phase relations are well characterized experimentally (to ~600 °C). There is, however, a fundamental thermodynamic anomaly in the NaCl–H_2O coexistence curve near the critical temperature of pure H_2O (Levelt Sengers et al., 1986; Harvey and Levelt Sengers, 1989; Anisimov et al., 2004) that may complicate extrapolation of partition coefficients across this region. This is most simply demonstrated by the "bird's beak" pattern in pressure-composition space for temperatures less than ~380 °C (Khaibullin and Borisov, 1966; Bischoff et al., 1986) that is also reproduced in our data from Exps. 7–8 (Fig. 8a). Given the low densities of NaCl saturated vapors are intuitively predicted to decrease with pressure, the result is a region for each isotherm where vapor chlorinity appears to increase with decreasing pressure/density (Fig. 8a). This, for example, effectively confounds the relationship of Eq. (7). Interpretation of data from Exps. 7–8 (363 °C) is therefore not straightforward because there is not a continuous decrease in chlorinity with decreasing pressure (density), and the attending change in M/Cl is intrinsically non-linear (Fig. 8b). It is for this reason these data were excluded when deriving the partition coefficients. When viewed in pressure-composition space, however, these data still show the general pattern of Fe > Zn > Mn in the vapor phase and the alkaline earths are very low in concentration. Thus, while the accuracy of either n or B values is less certain outside the experimentally calibrated range, use at higher temperatures seems likely to be less problematic.

In addition, we wish to emphasize that overall effects due to the presence of additional ligands (e.g., HS^-) and/or soluble minerals requires further constraint. For example, several recent investigations have concluded that vapor

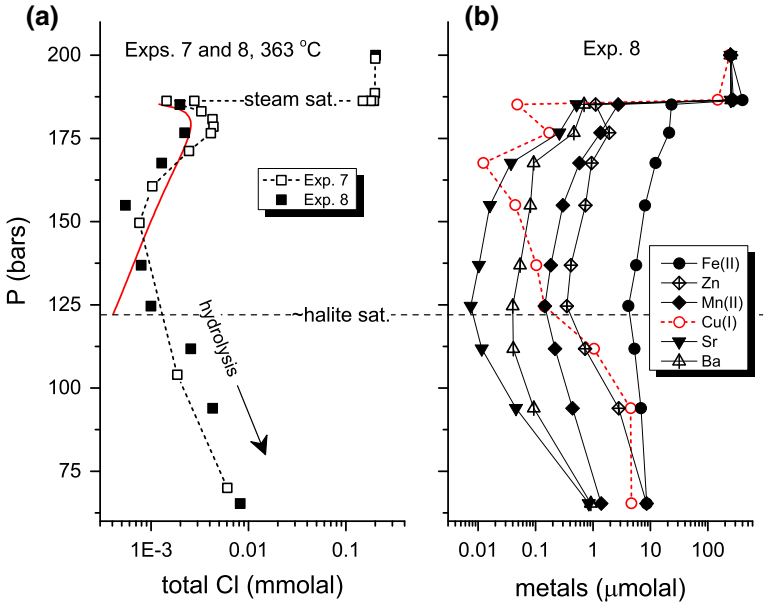

Fig. 8. (a) Vapor chlorinity with decreasing pressure at 363 °C from Exps. 7–8. Solid line corresponds to the model isotherm predicted by Driesner and Heinrich (2007). For temperatures near and below that of critical H_2O (373.9 °C) vapor chlorinity drops dramatically at the two-phase boundary (where $P \approx H_2O$ steam saturation for $T < 374$ °C and moderate bulk chlorinity) but subsequently increases before decreasing again with decreasing P, a phenomenon not observed at higher temperatures (see Fig. 2). This anomaly likely complicates the derivation of electrolyte partition coefficients at such temperatures (see Section 4.1). An increase in total chloride resulting from hydrolysis (Eq. (2)) at/near halite saturation is also observed in both experiments 7–8. (b) Vapor composition with decreasing pressure for Exp. 8. Metal concentrations drop substantially along with total chlorinity upon intersection of the two-phase boundary, see also panel (a). The general pattern observed in the higher temperature experiments (2–6) is evident with Fe > Zn > Mn > alkaline earths and increases in concentration associated with halite stability. These data show Ba > Sr and in some cases Ca (not shown for clarity). Cu concentrations initially drop dramatically but continuously increase with decreasing pressure to levels comparable to Fe and Zn, a pattern not exhibited by the other metals.

solubility of Fe and Zn is not appreciably enhanced by the presence of dissolved sulfide at geologically reasonable concentrations, whereas the effect on Cu and Au solubility may be substantial (Nagaseki and Hayashi, 2008; Pokrovski et al., 2008; Etschmann et al., 2010; Lerchbaumer and Audetat, 2012; Rempel et al., 2012).

4.2. Implications of speciation

Partitioning behavior of metals can be linked to the stability of aqueous species, specifically chloro-aqua complexes in the context of our experiments. In general, the extent of cation–anion association in electrolyte solutions increases with both increasing temperature and decreasing density due mainly to the concomitant decrease in the relative permittivity (dielectric constant) of water. Ideally we might compare our experimental data with thermodynamic calculations predicting the speciation of each metal in the vapors/liquids. However, due to challenging conditions, experimental data for apparent molal properties of electrolytes at near-critical or two-phase conditions are scarce (White et al., 1988; Majer et al., 1991); and even when available, extrapolation to infinite dilution in accordance with conventional asymmetric standard states and the Debye-Hückel limiting law can result in substantial error (Levelt Sengers et al., 1992). Similarly, thermodynamic formulations such as the revised HKF equation of state (Tanger and Helgeson, 1988; Shock et al., 1992) diverge anomalously in regions of high water compressibility ($\rho < \sim 0.6$ g/cm^3). Thus, our discussion is necessarily qualitative when applied to this region of P–T–x space.

4.2.1. Influence of ionic radius

The charge/radius ratio of both the cation and the anion are important factors governing the degree of hydration and ion pair formation (Pitzer, 1977; Fulton et al., 2006) and is a good starting point for comparison. Davies (1951), for example, has shown a strong linear relationship between this parameter and the association constants ($\log K_a$) of alkali and alkaline earth metal hydroxides in aqueous solution. Similarly, there is an excellent correlation between B constants and both the aqueous M–O internuclear distances (charge effects cancel out) and the dichloride (M–Cl) bond lengths for the alkaline earth metals (Fig. 9). Thus, for these metals, the partition coefficients agree with the suggestion that as water is replaced by a ligand of formal negative charge (e.g., Cl^-) the stability increment through purely electrostatic forces will increase with the reciprocal of the cationic radius (Irving and Williams, 1953). In other words, as the radii increase in the order Mg < Ca < Sr < Ba, stability of the associated chloro-complex should respectively decrease. Such a correlation (Fig. 9) is not surprising because spectroscopic studies show that while the number of hydration waters around a cation decreases with increasing T (decreasing density), the aqueous ionic radius remains essentially constant (e.g., Hoffmann et al., 1999; Seward and Driesner, 2004; Fulton et al., 2006). Yet, we have found no such simple correlation for the transition metals as the ionic radii are all quite similar; and though they do vary, they appear to do so systematically regardless of the coordination structure (octahedral, O_h, or tetrahedral, T_d, Fig. 9, see also next section). The stability/speciation of and bonding in transition metal complexes, however, is inherently different than for the alkali or alkaline earth elements because the partially filled d orbitals of transition elements may foster bonds that are partly covalent in nature (e.g., Shadle et al., 1995; Figgis and Hitchman, 2000). Regardless, the generality of correlation based on ionic radii is still evident as the transition metals all behave broadly similar to Mg (Fig. 9). A simple explanation for the lower partition coefficient of Fe is its unique ability to form abnormally strong complexes

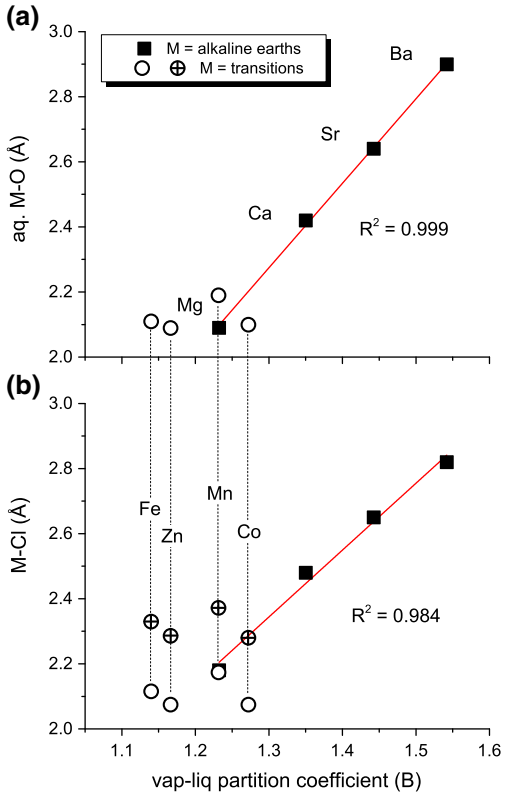

Fig. 9. Aqueous M–O bond distance (a) and M–Cl bond distance (b) for the divalent metals vs. associated vapor–liquid partition coefficients (B, Eq. (6)). M–O values are taken from Marcus (1988) where the ambient hydration shell consists of 6 water molecules for Mg and the transition metals (octahedral) and approximately 7, 8, 9 waters for Ca, Sr and Ba, respectively (Marcus, 1988; Seward et al., 1999; Fulton et al., 2003). An excellent linear correlation is observed for the alkaline earths. The transition metal M–Cl data represented by the crossed circles (b) are the average bond lengths in the tetrahedral $[MCl_4]^{2-}$ complex of crystalline $[N(CH_3)_4]_2{\cdot}[MCl_4]$ taken from Wiesner et al. (1967) and Lauher and Ibers (1975). All other M–Cl values are vapor-phase dichloride bond lengths where the molecules (MCl_2) are linear for Mg, Ca and the transitions but $SrCl_2$ and $BaCl_2$ are quasilinear and bent, respectively (Hargittai, 2000). A correlation for alkaline earths is still observed, though less robust than in panel (a). The transition metal data (connected by tie-lines to guide the eye) demonstrate the ionic radii vary systematically regardless of whether the coordination structure is octahedral, tetrahedral or linear.

relative to the other first-row transition metals (Irving and Williams, 1953; Gruen and McBeth, 1963).

4.2.2. Potentially dominant chloro-complexes

While systems of interest here have not yet been observed under two-phase conditions, spectroscopic studies have yielded great insight into speciation in high-temperature electrolyte solutions. In general, an increase in the extent of chloro-complexation under equivalent conditions can be described as; alkalis < alkaline earths < transition metals. Interestingly, though predicted by molecular dynamics simulations, contact ion pair formation was not resolved in 0.2–0.5 molal alkali-bromide solutions to temperatures as high as 450 °C and solution densities as low as ~0.4 g/cm^3, though a decrease (~40%) in waters of hydration was observed (Fulton et al., 1996; Ferlat et al., 2002). This contrasts with noteworthy ion pair formation for the divalent metals. For example, in ambient $CaCl_2$ solutions, there is no evidence of Cl^- within the first hydration shell of Ca^{2+} (species ≈ $[Ca(OH_2)_7]^{2+}$) at concentrations up to 6 molal, whereas, in a 1 molal solution at 400 °C, 350 bars, the ions are mostly associated, having a $CaCl_2^0/CaCl^+$ ratio of ~4 (Fulton et al., 2003, 2006; Badyal et al., 2004). For alkaline earths, excess chloride does not appear to significantly change the coordination structure or increase the extent of association (Fulton et al., 2006) and the predominant species may therefore be ~$[MCl_2(OH_2)_x]^0$.

Ion association equilibria is more complicated for transition elements due to enhanced bonding ability and a change from octahedral to tetrahedral coordination with increasing temperature/chlorinity. Furthermore, in NaCl dominated solutions, Na can act as a ligand donor to the metal center (Susak and Crerar, 1985; Hoffmann et al., 1999; Chen et al., 2005; Fulton et al., 2006). Dehydration across the coordination transition can therefore be represented by two end-members consisting of an ambient hexa-aqua complex and a high-temperature tetrachloro complex:

$$\overset{low\text{-}T,O_h}{[M(OH_2)_6]^{2+}} + 2Na^+ + 4Cl^- = 2Na^+\cdots\overset{high\text{-}T,T_d}{[MCl_4]^{2-}} + 6H_2O \quad (8)$$

where the Na^+ ions may be closely associated with the chloro complex assuming favorability of neutral species near criticality (Hoffmann et al., 1999; Mei et al., 2014). The exception is Cu(I) for which $CuCl_2^-$ (linear) appears most stable at high T (Fulton et al., 2000; Brugger et al., 2007). Regardless, Eq. (8) demonstrates transition metal speciation may be complicated, especially at moderate temperatures (~150–350 °C) where both octahedral and tetrahedral species might coexist (Susak and Crerar, 1985; Hoffmann et al., 1999; Migdisov et al., 2011). It is for this reason, for example, that interpretation of mineral solubility data in relation to the derivation of association constants is generally limited by the assumption of no higher order species than MCl_2^0 (e.g., for Fe(II), Ding and Seyfried, 1992; Fein et al., 1992). While such bulk values do not necessarily hinder metal solubility calculations at conditions associated with the experiments, unconstrained extrapolation of constants derived in this region to higher/lower temperatures or, conversely, extrapolation into this region, may be problematic. Therefore, so too may be the derivation of temperature/salinity independent partition coefficients for transition metals at moderate temperatures, further compounding issues related to the aforementioned thermodynamic anomaly for $T < 380$ °C (Section 4.1, Fig. 8).

While isothermally increasing salinity or decreasing pressure of a single-phase solution will have opposite effects on density, both will increase the extent of ion association (e.g., Mesmer et al., 1988; Oscarson et al., 2004). Therefore, upon phase separation, the drive for association will be further enhanced for all electrolytes in the resulting liquid. Under such low-pressure, high-chlorinity conditions, suggestions of more complex species (ionic clusters), though possible, become rather arbitrary (Anderko and Pitzer, 1993; Oelkers and Helgeson, 1993; Sedlbauer and Wood, 2004). The greatest uncertainties, especially for the transition metals, lie in the extent to which the dominant species in the vapor is equivalent to that in the liquid, and how speciation is affected by the NaCl/MCl_2 ratio relative to the H_2O/Cl ratio given also a dynamic range of density (e.g., Bazarkina et al., 2014). A relevant portion of the equilibria depicted in Eq. (8) may therefore be presented as:

$$2Na^+\cdots[MCl_4]^{2-} + 2H_2O = [MCl_2(OH_2)_2]^0 + 2NaCl^0 \quad (9)$$

where formation of trichloro and dichloro species may be increasingly favored with the increasing H_2O/Cl ratio in the vapor even though the bulk vapor NaCl/MCl_2 is greater than or equal to that in the coexisting liquid. For example, Liu et al. (2011) used spectral data to derive association constants (K_a values) for both $[CoCl_2(OH_2)_2]^0$ and $[CoCl_4]^{2-}$; and we have used these to calculate the distribution of aqueous species attending dilution of a 1 molal NaCl + 1 mmolal $CoCl_2$ solution with H_2O at 450 °C and 500 bars. The results show that $[CoCl_2(OH_2)_2]^0$ becomes the dominant Co(II) complex for $Cl_{tot} < 0.7$ molal. Though already at the limit of reliability for activity/concentration models, this condition is still far removed from the low-density vapors of interest here, and the diminished permittivity of H_2O may outweigh any increase in H_2O/NaCl ratios. Testemale et al. (2009) have similarly derived K_a values for $[FeCl_4]^{2-}$ and, at the specific P–T noted above, the log K_a for the Fe(II) species is ~30% higher than that of $[CoCl_4]^{2-}$. In a case where the tetrachloro complex is dominant in the vapor for both metals, this is consistent with the lower B values of Fe(II), and the more stable chloro-complex having a higher vapor affinity. Therefore, we do not rule out the possibility the partition coefficients can be proportional to ion association constants. Furthermore, our ability to empirically derive partition coefficients using formalisms rooted in the thermodynamic behavior of non-electrolytes (Eqs. (6), (7)) favors the idea that significant shifts in metal speciation are not occurring along most of the vapor–liquid solvus, and that the same (possibly fully associated) complex is dominant in both phases. However, more unusual patterns of volatility, such as enhanced solubility of Fe, Zn and Cu

at conditions less extreme than halite saturation (Figs. 4, S.5), could possibly reflect a shift in speciation (e.g., to the left in Eq. (9)). This is consistent with observed changes in the Fe isotopic composition of vapors collected during Exp. 4 (Syverson et al., 2014).

4.3. Phase separation in deep-sea hydrothermal systems

Time-series observations of hydrothermal fluid chemistry generally reveal short-lived periods of extremely low chlorinity concomitant with episodic magmatism (<1–2 years); and these events give way to significantly longer periods of steady-state hydrothermal circulation wherein vent fluids are moderately depleted to enriched in Cl relative to seawater (Von Damm et al., 1998; Lilley et al., 2003; Von Damm, 2004; Pester et al., 2012, 2014a). The results of our study allow us to assess with greater detail the potential role of phase separation in contributing to the chemical evolution of deep-sea hydrothermal fluids. The composition of dilute fluids associated with magmatic events (Von Damm, 2000, 2004; Lilley et al., 2003; Seewald et al., 2003; Seyfried et al., 2003; Fornari et al., 2012), for example, suggests vapor densities become sufficiently low that Fe exhibits volatile behavior (Pester et al., 2014a). Previous investigators have furthermore invoked subseafloor halite precipitation or dissolution in explanation of the significantly low Br/Cl ratios in vapors sampled during the 1991 eruptions on the East Pacific Rise (EPR, 9–10°N) (Oosting and Von Damm, 1996; Berndt and Seyfried, 1997; Von Damm, 2000). Such deviations in the Br/Cl ratio (relative to seawater) are seldom observed given both elements appear similarly conservative during hydrothermal alteration. However, the experimental data (Figs. 3, S.4) disagree with both scenarios involving halite because coincident with these low Br/Cl were pH (25 °C) values also atypically low for EPR vent fluids. Active halite precipitation should otherwise produce acidic vapors (via hydrolysis) with high Br/Cl, whereas dissolution of alkaline (NaOH-bearing), potentially Br-depleted halite would have similarly inverse effects. Thus, though still possible, vapors bearing chemistry fully consistent with subseafloor halite saturation have yet to be recovered.

Barring magmatic intrusions, phase separation during more steady-state periods appears to be occurring at P–T conditions near the critical curve in accordance with the physical properties of the fluids (Norton, 1984; Jupp and Schultz, 2000; Driesner and Geiger, 2007; Pester et al., 2014a). Intersection of the two-phase boundary is likely a fundamental driver of hydrothermal circulation and ridge-axis venting. However, logistical issues still exist regarding the persistent emanation of Cl-depleted fluids from many intermediate to fast spreading ridge segments because build-up of a stably-stratified (subseafloor) brine layer should eventually shut down the convection cell; and off- or along-axis migration of Cl-rich brines may be required (Fontaine and Wilcock, 2006; Larson et al., 2009; Pester et al., 2011). Conversely, Cl-depleted fluids appear distinctly absent from many slower spreading ridges (Mid-Atlantic Ridge, MAR, and Central Indian Ridge, CIR). Though certainly unconstrained, this suggests another mechanism such as mineral hydration might contribute "pre-enriched" fluids to the main hydrothermal circulation cell. For example, slow spreading ridges may have broader and deeper recharge zones that incorporate a fluid flux modified by integrated serpentinization of more distal ultramafic lithologies. Nonetheless, the Fe/Mn ratios in many Cl-enriched vent fluids reflect temperatures that fall within the vapor field of the two-phase envelope (Pester et al., 2011, 2014b). Despite having chlorinity higher than seawater, this suggests these fluids still represent a vapor phase, having been derived from an even higher chlorinity source fluid. We therefore explicitly consider this scenario when evaluating vent data in the context of vapor–liquid partitioning (e.g., fluids from 13°N, EPR, and Kairei-Edmond, CIR, see below). However, given sampling heterogeneity and the complexity of natural systems, the extent to which data at any given spatial (ridge system, segment, or vent field) or temporal scale may be assumed to result from the same or similar chemical/physical forcings is uncertain.

4.3.1. The example of Ca: phase separation vs. fluid-mineral equilibria

Calcium has one of the higher partition coefficients, and its solubility appears much less sensitive to modest changes in temperature than any of the transition metals (Berndt et al., 1989; Seewald and Seyfried, 1990; Seyfried et al., 2002; Pester et al., 2012). This makes it more likely to reflect/preserve the effects of phase separation; and this process is a possible explanation for the general increase in Ca/Cl ratios with chlorinity in natural vent fluids. One way to quickly evaluate agreement with partitioning behavior is to observe statistical output (e.g., R^2, confidence bands) when data are treated in a manner similar to Fig. 5, but the slope of the regression (S_V) is forced to correspond to the metal in question. This most simple methodology inherently presumes all vent fluids included in the fit are variably saline vapors derived from the same or similar source fluid(s), and, for example, the Ca–Cl relationships from both EPR, 13°N (Fig. 10a) and Kairei-Edmond (CIR, Fig. 10b) are contextually consistent. Similarly, data from Fenway (PACMANUS, Fig. 10c) may reflect phase separation of a fluid having near seawater chlorinity, with the Cl-enriched fluid representing a conjugate liquid. We note Fig. 10a and b in particular because the data of EPR, 13°N encompass samples acquired within close proximity, but separated in time of sampling by 25 years, and, while the CIR fluids are venting from compositionally similar (basaltic) substrate, the Kairei and Edmond vent fields are located ~160 km apart (Gallant and Von Damm, 2006; Kumagai et al., 2008). Thus, to attribute the observed relationships solely to the effects of phase separation is tenuous given also potential mineral solubility effects.

Only in the laboratory can we unambiguously isolate the effects of chloride variability on fluid-mineral equilibria relative to the effects of phase separation (vapor–liquid equilibria). We therefore attempt a comparison between the vapor–liquid fractionation of Ca and an empirical model for plagioclase solubility (Pester et al., 2012) derived using the combined experimental data of Berndt and Seyfried

(1993) and Seyfried et al. (2002). These solubility experiments were conducted at temperatures specifically relevant to mid-ocean ridge hydrothermal systems (400–425 °C) but at pressures sufficiently high that the fluids were maintained as a single phase (300–500 bars). These data demonstrate that, for any given plagioclase (solid solution) composition, the dissolved Ca/Cl ratio will increase with total chlorinity in NaCl dominated solutions. Accordingly, this is another possible explanation for the broader Ca–Cl systematics observed in vent fluids (where $Cl \approx 2*Ca + Na$, Fig. 11). Remarkable, however, is that this empirical solubility relationship reproduces well the predicted change in a vapor's Ca/Cl ratio under variable extents of phase separation (Fig. 11a). Therefore, vent data consistent with a single vapor-partitioning curve for Ca (e.g., Fig. 10) will inherently also be consistent with a given plagioclase solubility curve. For example, Fig. 11a suggests phase separation of a fluid initially with seawater chlorinity and in equilibrium with An70 can produce a vapor with compositional characteristics that are difficult to resolve from the An70 (mineral-fluid) solubility curve. In contrast, the evolved liquids retain Ca/Cl ratios similar to the initial single-phase solution, departing from the An70 curve. The fate of these liquids (e.g., L1, Fig. 11a) would likely involve longer residence times in the crust where they may or may not re-equilibrate with the host lithology before encountering again the two-phase boundary at a higher temperature. We recognize the broad uncertainty in arbitrarily intermingling two empirical models derived (necessarily) at somewhat different chemical/physical conditions, and do not imply such a model is quantitatively representative of integrated subseafloor processes. Nonetheless, Fig. 11 demonstrates how either single or multiple episodes of phase separation, with or without subsequent re-equilibration with ~An70, might account for most of the EPR vent fluid compositions. Further information is required if, for example, we wish to explore whether or not the Cl-enriched and Cl-depleted fluids from EPR, 13°N (Figs. 10a, 11) evolved via phase separation of the same parent liquid. Interestingly, the Cl-enriched fluids recovered in 2008 had ~3× more dissolved CO_2 than the nearby Cl-depleted fluids, ruling out this scenario and suggesting the possibility of either different source fluids or multiple episodes of phase separation (Pester et al., 2011).

Finally, we note that within the broader context of hydrothermal fluid compositions (Fig. 11b), the extent to which a given plagioclase solid solution quantitatively reproduces Ca solubility associated with bulk basalt alteration is still uncertain. Experiments demonstrate basalt crystallinity may be a significant influence on appreciable timescales, where increasing crystallinity (more diabasic) decreases dissolved Ca (Mottl and Holland, 1978; Berndt et al., 1989). Furthermore, the magnitude of temperature effects increases with decreasing crystallinity. Regardless, for a fixed chlorinity, the magnitude/range of the Ca/Cl ratio(s) observed in vent fluids can be summarily explained within these contexts (Fig. 11b). The similarity in Ca–Cl systematics predicted by the (vapor) phase separation and

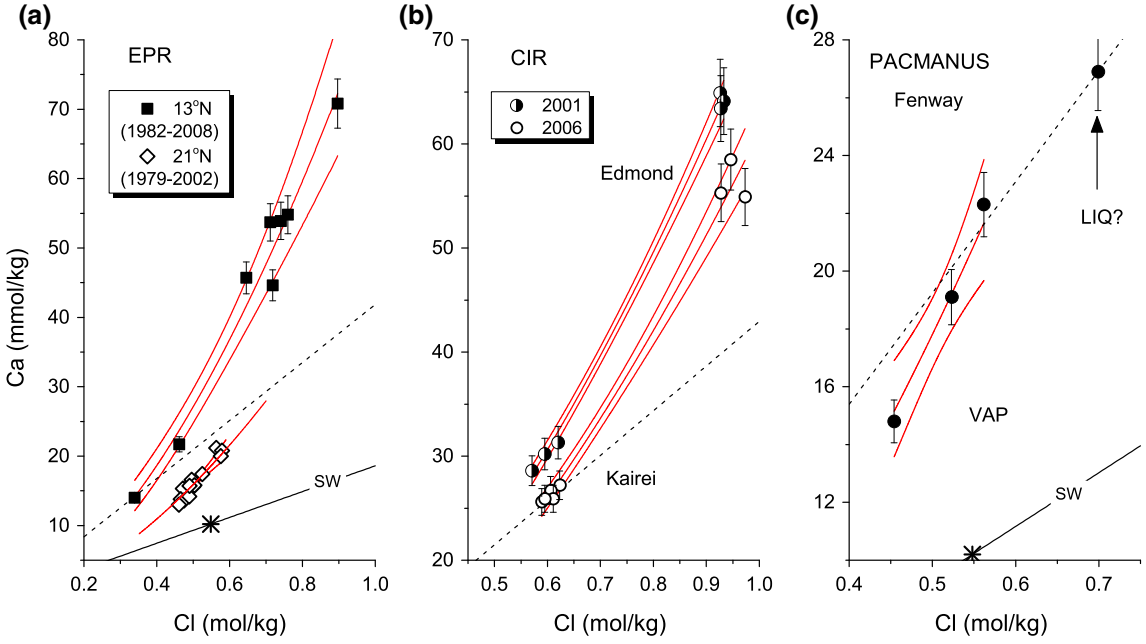

Fig. 10. Dissolved Ca vs. Cl in hydrothermal vent fluids from selected sites. Data are regressed in a manner similar to Fig. 5 (S_V, Eq. (4)) but require the slope correspond to the Ca partition coefficient ($S_V = 0.639$). Shown here, fit results (and 95% confidence bands) have been translated into linear (axes) elemental plots for data from (a) EPR, 13°N (Grimaud et al., 1984; Michard et al., 1984; Pester et al., 2011) and EPR, 21°N (Von Damm et al., 1985a; Von Damm et al., 2002) (fit line extended for clarity, exempting data from Hanging Gardens), (b) Kairei and Edmond, CIR (Gallant and Von Damm, 2006; Kumagai et al., 2008), and (c) PACMANUS (Fenway vents), Pual Ridge (Reeves et al., 2011). Only fluids with exit temperatures > 250 °C are considered. Error bars show most data agree with Ca (vapor) partitioning within 5%. A solid line depicts the Ca/Cl ratio of seawater (hatched symbol, a, c). Additional (dashed) lines of fixed Ca/Cl ratios are shown for reference, though that in panel (c) is placed to suggest the possibility the Cl-enriched fluid represents a conjugate liquid.

plagioclase solubility models suggests that, for any given sequence of chemical and physical factors, it may be difficult to unambiguously unravel the relative significance of each process on the compositional evolution of hydrothermal fluids. We emphasize, however, that while evolving vapors leave the system to vent at the seafloor, the residual liquids left behind may, for many metals, be persistently undersaturated with respect to the surrounding mineralogy (e.g., L1, Fig. 11a), providing a mechanism that continuously drives hydrothermal alteration. In this case, the process of phase separation coupled with phase segregation may actually enhance the rate and/or extent of alteration. More importantly there still exists the possibility of a fundamental link between quantitative vapor–liquid partition coefficients and the relative stability of dominant aqueous complexes that ultimately affect mineral solubility.

5. SUMMARY AND CONCLUSIONS

We have derived both chloride and density dependent vapor–liquid partition coefficients for alkaline earth and first row transition metals in NaCl dominated fluids. Elements are normalized to Na = 1, this being the cation that most dictates phase behavior in natural hydrothermal systems. Statistically robust relationships indicate decreasing affinity for the vapor phase in the order Cu(I) > Na > Fe(II) > Zn > Ni(II) ≳ Mg ≳ Mn(II) > Co(II) > Ca > Sr > Ba. These values should accurately describe compositional variability in coexisting vapors and liquids at temperatures between ~380 and 600 (+) °C for vapor density > ~0.2 g/cm^3. Data from experiments conducted at 360 °C did not give consistent results, which might be expected given the known thermodynamic anomalies in the NaCl–H_2O coexistence curves for temperatures near and below the critical point of pure H_2O.

The four alkaline earth elements exhibit a linear correlation ($R^2 > 0.99$) between their partition coefficients and respective aqueous ionic radii, reflecting purely electrostatic interactions with chloride ligands. Such a relationship is not conclusive for the transitions metals, due likely to more complex bonding and coordination structures. It is, nonetheless, possible the partition coefficients are proportional to related ion association constants, with implications for near-critical mineral solubility. Such a development would indeed facilitate implementation of multi-phase/component reactive transport models at challenging hydrothermal conditions.

Representative vapor–liquid partitioning gives way to opposing, non-linear behavior as the halite stability field is approached, where vapor *M*/Cl ratios begin to increase

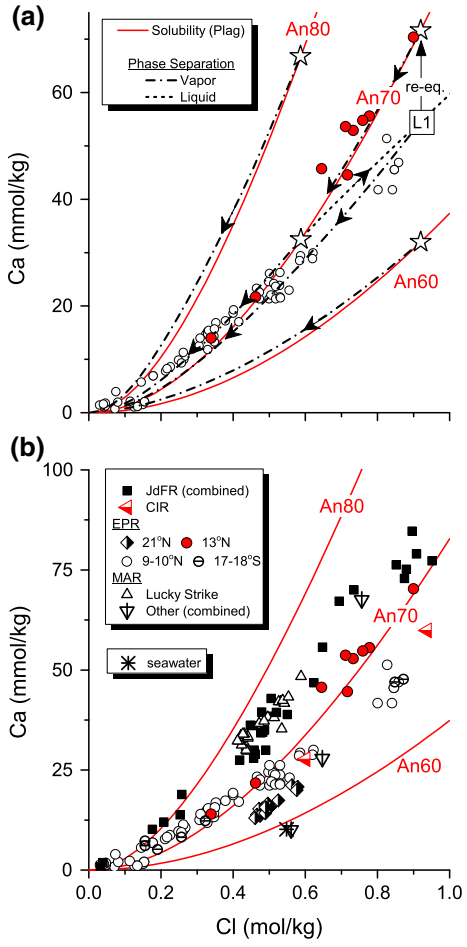

Fig. 11. Dissolved Ca vs. Cl in hydrothermal vent fluids in the context of plagioclase solubility. The empirical relationship $\log(mCa^{2+}/m^2Na^{+}) = 0.0435\ (x_{An}) - 6.97$ predicts the dissolved Ca/Na ratio (2*Ca + Na = Cl) in equilibrium with a given plagioclase solid-solution (x_{An} = % anorthite) at temperatures consistent with subseafloor hydrothermal alteration (Pester et al., 2012). Relationships for An80, An70 and An60 are given (solid curves). Panel (a) superimposes modeled phase separation scenarios on the mineral solubility curves. Phase separation curves were calculated using Eq. (5) and mass balance Eqs. S.1–S.3 as described in Supplementary Materials. Star symbols represent (starting) fluid compositions in equilibrium with a given plagioclase. The Ca concentrations of lower chlorinity vapors generated via phase separation follow closely the associated solubility curves. For reference, the difference between the vapor and plagioclase curves is on the order of that between the Ca and Sr partition coefficients. Liquid compositions are not shown for the An80 and An60 examples. The An70 model is multifaceted where phase separation of an equilibrated fluid with seawater chlorinity (at 410 °C) produces liquids along a trajectory including L1. Prior to a second phase separation event (at 425 °C) L1 may or may not re-equilibrate with An70. The latter scenario is consistent with data from EPR, 9–10°N whereas the former is consistent with EPR, 13°N. Panel (b), a compendium of vent data (Grimaud et al., 1984; Michard et al., 1984; Von Damm et al., 1985a, 1998, 2002; Campbell et al., 1988; Butterfield et al., 1990, 1994, 1997; Butterfield and Massoth, 1994; Edmond et al., 1995; Charlou et al., 1996, 2000, 2002; Von Damm, 2000, 2004; Seyfried et al., 2003, 2011; Gallant and Von Damm, 2006; Foustoukos and Seyfried, 2007b; Kumagai et al., 2008; Foustoukos et al., 2009; Pester et al., 2011, 2012). Combined data from Juan de Fuca Ridge represent Main Endeavour, Axial (ASHES), Coaxial and Cleft segments. Additional MAR sites (averaged values given temporally stable composition) vary from near seawater (MARK, 23°N) to the more enriched fluids of TAG (26°N) and Rainbow (36°N), respectively. Kairei and Edmond fluids (CIR) are also averaged for clarity (see Fig. 10b).

despite continued decreases in vapor chlorinity/density. This "volatility" is broadly concomitant with substantial increases in the HCl/NaCl ratio (eventually to >1) due to hydrolysis of NaCl. The chemistry of deep-sea hydrothermal fluids collected during seafloor eruptions suggests the short term evolution of sufficiently low-density vapors that certain transition metals will exhibit volatile behavior (e.g., Fe). However, experimental results do not fully agree with inferences that these vapors reflect halite precipitation/dissolution processes.

The Ca–Cl systematics in fluids representative of more steady-state (longer term) hydrothermal circulation inevitably reflect integrated effects of both phase separation and mineral alteration. Empirical models that isolate the effects of both processes surprisingly reveal that changes in the relative distribution of Ca and Cl in an evolving vapor (phase separation only) are similar to changes in the Ca/Cl ratio with total chlorinity imposed by mineral (plagioclase) solubility. Because vent fluids sampled at the seafloor generally represent the more buoyant vapor phase, it appears difficult to gauge the relative contribution of each process to the measured chemical compositions (noting also field samples are generally consistent with both processes/models). The compared models do, however, suggest phase separation and concomitant phase segregation may result in the continuous production of undersaturated residual liquids, enhancing the rate and extent of subseafloor hydrothermal alteration.

ACKNOWLEDGEMENTS

We thank Rick Knurr for analysis of the experimental samples, Shijun Wu for drafting Fig. 1, and Robert Jones for helping fabricate the new Ti-alloy reaction vessel. Thoughtful comments from Gleb Pokrovski, Axel Liebscher and two anonymous reviewers greatly improved the clarity and content of the manuscript. Financial support for this research was provided by NSF grants 0927615, 0751771, 0813861 (WES, KD).

APPENDIX A. SUPPLEMENTARY DATA

Supplementary data associated with this article can be found, in the online version, at http://dx.doi.org/10.1016/j.gca.2015.07.028.

REFERENCES

Alt J. C., Laverne C., Coggon R. M., Teagle D. A. H., Banerjee N. R., Morgan S., Smith-Duque C. E., Harris M. and Galli L. (2010) Subsurface structure of a submarine hydrothermal system in ocean crust formed at the East Pacific Rise, ODP/IODP Site 1256. *Geochem. Geophys. Geosyst.* **11**, Q10010, doi:10010.11029/12010GC003144.

Alvarez J., Corti H. R., Fernandez-Prini R. and Japas M. L. (1994) Distribution of solutes between coexisiting steam and water. *Geochim. Cosmochim. Acta* **58**, 2789–2798.

Anderko A. and Pitzer K. S. (1993) Equation of state representation of phase equilibria and volumetric properties of NaCl–H_2O above 573 °C. *Geochim. Cosmochim. Acta* **57**, 1657–1680.

Anisimov M. A., Sengers J. V. and Levelt Sengers J. M. H. (2004) Near-critical behavior of aqueous systems. In *Aqueous Systems at Elevated Temperatures and Pressures* (eds. D. A. Palmer, R. Fernandez-Prini A. H. Harvey). Elsevier, pp. 29–71.

Armellini F. J. and Tester J. W. (1993) Solubility of sodium chloride and sulfate in sub- and supercritical water vapor from 450–550 °C and 100–250 bar. *Fluid Phase Equilib.* **84**, 123–142.

Arnorsson S., Stefansson A. and Bjarnason J. O. (2007). Fluid–fluid interactions in geothermal systems. In *Fluid–Fluid Interactions, Rev. Mineral. Geochem. 65* (eds. A. Liebscher, C. A. Heinrich). MSA, Chantilly, VA. pp. 259–312.

Badyal Y. S., Barnes A. C., Cuello G. J. and Simonson J. M. (2004) Understanding the effects of concentration on the solvation structure of Ca^{2+} in aqueous solution. II: insights into longer range order from neutron diffraction isotope substitution. *J. Phys. Chem. A* **108**, 11819–11827.

Bazarkina E. F., Pokrovski G. S. and Hazemann J. L. (2014) Structure, stability and geochemical role of palladium chloride complexes in hydrothermal fluids. *Geochim. Cosmochim. Acta* **146**, 107–131.

Berndt M. E. and Seyfried, Jr., W. E. (1990) Boron, bromine, and other trace elements as clues to the fate of chlorine in mid-ocean ridge vent fluids. *Geochim. Cosmochim. Acta* **54**, 2235–2245.

Berndt M. E. and Seyfried, Jr., W. E. (1993) Calcium and sodium exchange during hydrothermal alteration of calcic plagioclase at 400 °C and 400 bars. *Geochim. Cosmochim. Acta* **57**, 4445–4451.

Berndt M. E. and Seyfried, Jr., W. E. (1997) Calibration of Br/Cl fractionation during subcritical phase separation of seawater; possible halite at 9 to 10°N East Pacific Rise. *Geochim. Cosmochim. Acta* **61**, 2849–2854.

Berndt M. E., Seyfried, Jr., W. E. and Janecky D. R. (1989) Plagioclase and epidote buffering of cation ratios in mid-ocean ridge hydrothermal fluids: experimental results in and near the supercritical region. *Geochim. Cosmochim. Acta* **53**, 2283–2300.

Berndt M. E., Seal, II, R. R., Shanks, III, W. C. and Seyfried, Jr., W. E. (1996) Hydrogen isotope systematics of phase separation in submarine hydrothermal systems: experimental calibration and theoretical models. *Geochim. Cosmochim. Acta* **60**, 1595–1604.

Bischoff J. L. (1991) Densities of liquids and vapors in boiling NaCl–H_2O solutions: A PVTx summary from 300° to 500 °C. *Am. J. Sci.* **291**, 309–338.

Bischoff J. L. and Pitzer K. S. (1989) Liquid–vapor relations for the system NaCl–H_2O: summary of the P–T–x surface from 300°C to 500 °C. *Am. J. Sci.* **289**, 217–248.

Bischoff J. L. and Rosenbauer R. J. (1984) The critical point and two-phase boundary of seawater, 200–500 °C. *Earth Planet. Sci. Lett.* **68**, 172–180.

Bischoff J. L. and Rosenbauer R. J. (1985) An empirical equation of state for hydrothermal seawater (3.2% NaCl). *Am. J. Sci.* **285**, 725–763.

Bischoff J. L. and Rosenbauer R. J. (1987) Phase separation in seafloor geothermal systems: an experimental study on the effects of metal transport. *Am. J. Sci.* **287**, 953–978.

Bischoff J. L. and Rosenbauer R. J. (1988) Liquid–vapor relations in the critical region of the system NaCl–H_2O from 380 to 415 °C: a refined determination of the critical point and two-phase boundary of seawater. *Geochim. Cosmochim. Acta* **52**, 2121–2126.

Bischoff J. L., Rosenbauer R. J. and Pitzer K. S. (1986) The system NaCl–H_2O: relations of vapor–liquid near the critical temperature of water and of vapor–liquid–halite from 300° to 500 °C. *Geochim. Cosmochim. Acta* **50**, 1437–1444.

Bischoff J. L., Rosenbauer R. J. and Fournier R. O. (1996) The generation of HCl in the system $CaCl_2$–H_2O: vapor–liquid relations from 380 to 500 °C. *Geochim. Cosmochim. Acta* **60**, 7–16.

Bodnar R. J., Burnham C. W. and Sterner S. M. (1985) Synthetic fluid inclusions in natural quartz. III. Determination of phase equilibrium properties in the system H_2O–NaCl to 1000 °C and 1500 bars. *Geochim. Cosmochim. Acta* **49**, 1861–1873.

Brugger J., Etschmann B., Liu W., Testemale D., Hazemann J. L., Emerich H., van Beek W. and Proux O. (2007) An XAS study of the structure and thermodynamics of Cu(I) chloride complexes in brines up to high temperature (400 C, 600 bar). *Geochim. Cosmochim. Acta* **71**, 4920–4941.

Butterfield D. A. and Massoth G. J. (1994) Geochemistry of north Cleft segment vent fluids: temporal changes in chlorinity and their possible relation to recent volcanism. *J. Geophys. Res.* **99**, 4951–4968.

Butterfield D. A., Massoth G. J., McDuff R. E., Lupton J. E. and Lilley M. D. (1990) Geochemistry of hydrothermal fluids from Axial Seamount Hydrothermal Emissions Study vent field, Juan de Fuca Ridge: Subseafloor boiling and subsequent fluid–rock interaction. *J. Geophys. Res.* **95**, 12895–12921.

Butterfield D. A., McDuff R. E., Mottl M. J., Lilley M. D., Lupton J. E. and Massoth G. J. (1994) Gradients in the composition of hydrothermal fluids from the Endeavor Segment vent field: Phase separation and brine loss. *J. Geophys. Res.* **99**, 9561–9583.

Butterfield D. A., Jonasson I. R., Massoth G. J., Feely R. A., Roe K. K., Embley R. W., Holden J. F., McDuff R. E., Lilley M. D. and Delaney J. R. (1997) Seafloor eruptions and evolution of hydrothermal fluid chemistry. *Phil. Trans. R. Soc. Lond. A* **355**, 369–386.

Campbell A. C., Palmer M. R., Klinkhammer G. P., Bowers T. S., Edmond J. M., Lawrence J. R., Casey J. F., Thompson G., Humphris S., Rona P. and Karson J. A. (1988) Chemistry of hot springs on the Mid-Atlantic Ridge. *Nature* **335**, 514–519.

Charlou J. L., Fouquet Y., Donval J. P., Auzende J. M., Jean-Baptiste P. and Stievenard M. (1996) Mineral and gas chemistry of hydrothermal fluids on an ultrafast spreading ridge: East Pacific Rise, 17° to 19°S (Naudur cruise, 1993) phase separation processes controlled by volcanic and tectonic activity. *J. Geophys. Res.* **101**(15), 899–815, 919.

Charlou J. L., Donval J. P., Douville E., Jean-Baptiste P., Radford-Knoery J., Fouquet Y., Dapoigny A. and Stievenard M. (2000) Compared geochemical signatures and the evolution of Menez Gwen (37°50′N) and Lucky Strike (37°17′N) hydrothermal fluids, south of the Azores Triple Junction on the Mid-Atlantic Ridge. *Chem. Geol.* **171**, 49–75.

Charlou J. L., Donval J. P., Fouquet Y., Jean-Baptiste P. and Holm N. (2002) Geochemistry of high H_2 and CH_4 vent fluids issuing from ultramafic rocks at the Rainbow hydrothermal field (36°14′N, MAR). *Chem. Geol.* **191**, 345–359.

Chen Y., Fulton J. L. and Partenheimer W. (2005) The structure of the homogenous oxidation catalyst, $Mn(II)(Br^{-1})_x$, in supercritical water: an X-ray absorption fine-structure study. *J. Am. Chem. Soc.* **127**, 14085–14093.

Coombs M. L., Sisson T. W. and Kimura J. (2004) Ultra-high chlorine in submarine Kilauea glasses: evidence for direct assimilation of brine by magma. *Earth Planet. Sci. Lett.* **217**, 297–313.

Crerar D., Wood S., Brantley S. and Bocarsly A. (1985) Chemical controls on solubility of ore-forming minerals in hydrothermal solutions. *Can. Mineral.* **23**, 333–352.

Davies C. W. (1951) The electrolytic dissociation of metal hydroxides. *J. Chem. Soc.*, 1256–1258.

Ding K. and Seyfried, Jr., W. E. (1992) Determination of Fe–Cl complexing in the low pressure supercritical region (NaCl fluid): iron solubility constraints on pH of subseafloor hydrothermal fluids. *Geochim. Cosmochim. Acta* **56**, 3681–3692.

Douville E., Charlou J. L., Oelkers E. H., Bienvenu P., Jove Colon C. F., Donval J. P., Fouquet Y., Prieur D. and Appriou P. (2002) The rainbow vent fluids (36°14′N, MAR): the influence of ultramafic rocks and phase separation on trace metal content in Mid-Atlantic Ridge hydrothermal fluids. *Chem. Geol.* **184**, 37–48.

Driesner T. (2007) The system H_2O–NaCl. Part II: correlations for molar volume, enthalpy, and isobaric heat capacity from 0 to 1000 °C, 1 to 5000 bar, and 0 to $1\times_{NaCl}$. *Geochim. Cosmochim. Acta* **71**, 4902–4919.

Driesner T. and Geiger S. (2007) Numerical simulation of multiphase fluid flow in hydrothermal systems. In *Fluid–Fluid Interactions* (eds. A. Liebscher, C. A. Heinrich). Rev. Mineral. Geochem. 65. MSA, Chantilly, VA. pp. 187–212.

Driesner T. and Heinrich C. A. (2007) The system H_2O–NaCl. Part I: correlation formulae for phase relations in temperature-pressure-composition space from 0 to 1000 °C, 0 to 5000 bar, and 0 to $1\times_{NaCl}$. *Geochim. Cosmochim. Acta* **71**, 4880–4901.

Drummond S. E. and Ohmoto H. (1985) Chemical evolution and mineral deposition in boiling hydrothermal systems. *Econ. Geol.* **80**, 126–147.

Edmond J. M., Campbell A. C., Palmer M. R., Klinkhammer G. P., German C. R., Edmonds H. N., Elderfield H., Thompson G. and Rona P. (1995) Time series studies of vent fluids from the TAG and MARK sites (1986, 1990) Mid-Atlantic Ridge: a new solution chemistry model and a mechanism for Cu/Zn zonation in massive sulphide orebodies. In *Hydrothermal Vents and Processes, Geo. Soc. Spec. Pub. No. 87*. (eds. L. M. Parson, C. L. Walker, D. R. Dixon). The Geological Society, London. pp. 77–86.

Etschmann B. E., Liu W., Testemale D., Muller H., Rae N. A., Proux O., Hazemann J. L. and Brugger J. (2010) An in situ XAS study of copper(I) transport as hydrosulfide complexes in hydrothermal solutions (25–592 °C, 180–600 bar): speciation and solubility in vapor and liquid phases. *Geochim. Cosmochim. Acta* **74**, 4723–4739.

Fein J. B., Hemley J. J., D' Angelo W. M., Komninou A. and Sverjensky D. A. (1992) Experimental study of iron-chloride complexing in hydrothermal fluids. *Geochim. Cosmochim. Acta* **56**, 3179–3190.

Ferlat G., San Miguel A., Jal J. F., Soetens J. C., Bopp P. A., Hazemann J. L., Testemale D. and Daniel I. (2002) The quest for ion pairing in supercritical aqueous electrolytes. *J. Mol. Liq.* **101**, 127–136.

Fernandez-Prini R., Japas M. L. and Corti H. R. (1993) Thermodynamics of high temperature electrolyte solutions: vapour–liquid equilibrium. *Pure Appl. Chem.* **65**, 913–918.

Fernandez-Prini R., Alvarez J. L. and Harvey A. H. (2003) Henry's constants and vapor–liquid distribution constants for gaseous solutes in H_2O and D_2O at high temperatures. *J. Phys. Chem. Ref. Data* **32**, 903–916.

Figgis B. N. and Hitchman M. A. (2000) *Ligand Field Theory and Its Applications*. Wiley-VCH.

Fontaine F. J. and Wilcock W. S. (2006) Dynamics and storage of brine in mid-ocean ridge hydrothermal systems. *J. Geophys. Res.* **111**, B06102. http://dx.doi.org/10.1029/2005JB003866.

Fontaine F. J., Wilcock W. S., Foustoukos D. I. and Butterfield D. A. (2009) A Si-Cl geothermobarometer for the reaction zone of high-temperature, basaltic-hosted mid-ocean ridge hydrothermal systems. *Geochem. Geophys. Geosyst.* **10**, Q05009, Doi:05010.01029/02009GC002407.

Fornari D. J., Von Damm K. L., Bryce J. G., Cowen J. P., Ferrini V., Fundis A., Lilley M. D., Luther, III, G. W., Mullineaux L. S., Perfit M. R., Meana-Prado M. F., Rubin K. H., Seyfried, Jr., W. E., Shank T. M., Soule S. A., Tolstoy M. and White S. M. (2012) The East Pacific Rise between 9 N

and 10 N: twenty-five years of integrated, multidisciplinary oceanic spreading center studies. *Oceanography* **25**, 18–43.

Fournier R. O. and Thompson J. M. (1993) Composition of steam in the system NaCl–KCl–H_2O–quartz at 600 °C. *Geochim. Cosmochim. Acta* **57**, 4365–4375.

Foustoukos D. I., Seyfried W. E., Jr. (2007a) Fluid phase separation processes in submarine hydrothermal systems. In *Fluid-Fluid Interactions* (eds. A. Liebscher, C. A. Heinrich). Rev. Mineral. Geochem. 65. MSA, Chantilly, VA. pp. 213–239.

Foustoukos D. I. and Seyfried, Jr., W. E. (2007b) Quartz solubility in the two-phase and critical region of the NaCl–KCl–H_2O system: implications for submarine hydrothermal vent systems at 9°50′N East Pacific Rise. *Geochim. Cosmochim. Acta* **71**, 186–201.

Foustoukos D. I. and Seyfried, Jr., W. E. (2007c) Trace element partitioning between vapor, brine and halite under extreme phase separation conditions. *Geochim. Cosmochim. Acta* **71**, 2056–2071.

Foustoukos D. I., Pester N. J., Ding K. and Seyfried, Jr., W. E. (2009) Dissolved carbon species in associated diffuse and focused flow hydrothermal vents at the Main Endeavour Field, Juan de Fuca Ridge: phase equilibria and kinetic constraints. *Geochem. Geophys. Geosyst.* **10**, Q10003, doi:10010.11029/12009GC002472.

Fulton J. L., Pfund D. M., Wallen S. L., Newville M., Stern E. A. and Ma Y. (1996) Rubidium ion hydration in ambient and supercritical water. *J. Phys. Chem.* **105**, 2161–2166.

Fulton J. L., Hoffmann M. M., Darab J. G., Palmer B. J. and Stern E. A. (2000) Copper(I) and copper(II) coordination structure under hydrothermal conditions at 325 °C: an X-ray absorption fine structure and molecular dynamics study. *J. Phys. Chem. A* **104**, 11651–11663.

Fulton J. L., Heald S. M., Badyal Y. S. and Simonson J. M. (2003) Understanding the effects of concentration on the solvation structure of Ca^{2+} in aqueous solution. I: the perspective on local structure from EXAFS and XANES. *J. Phys. Chem. A* **107**, 4688–4696.

Fulton J. L., Chen Y., Heald S. M. and Balasubramanian M. (2006) Hydration and contact ion pairing of Ca^{2+} with Cl^- in supercritical aqueous solution. *J. Chem. Phys.*, 094507.

Gallant R. M. and Von Damm K. L. (2006) Geochemical controls on the hydrothermal fluids from the Kairei and Edmond Vent Fields, 23°–25°S. Central Indian Ridge. *Geochem. Geophys. Geosyst.* **7**, Q06018.

German C. R. a nd Seyfried W. E., Jr. (2014) Hydrothermal processes. In *Treatise on Geochemistry, Vol. 8* (ed S. A. Elias). The Oceans and Marine Geochemistry. Elsevier. pp. 191–233.

Giggenbach W. F. (1997) The origin and evolution of fluids in magmatic-hydrothermal systems. In *Geochemistry of Hydrothermal Ore Deposits, 3rd ed.* (ed. H. L. Barnes). John Wiley & Sons Inc. pp. 737–796.

Gillis K. M. (1995) Controls on hydrothermal alteration in a section of fast-spreading oceanic crust. *Earth Planet. Sci. Lett.* **134**, 473–489.

Grimaud D., Michard A. and Michard G. (1984) Composition chimique et composition isotopique du strontium dans les eaux hydrothermales sous-marines de la dorsale Est Pacifique a 13° Nord. *C. R. Acad. Sci. Paris* **299**, 865–870.

Gruen D. M. and McBeth R. L. (1963) The coordination chemistry of 3d transition metal ions in fused salt solutions. *Pure Appl. Chem.* **6**, 23–47.

Hargittai M. (2000) Molecular structure of metal halides. *Chem. Rev.* **100**, 2233–2301.

Harvey A. H. and Levelt Sengers J. M. H. (1989) On the NaCl–H_2O coexistence curve near the critical temperature of H_2O. *Chem. Phys. Lett.* **156**, 415–417.

Heinrich C. A., Gunther D., Audetat A., Ulrich T. and Frischknecht R. (1999) Metal fractionation between magmatic brine and vapor, determined by microanalysis of fluid inclusions. *Geology* **27**, 755–758.

Ho P. C., Palmer D. A. and Gruszkiewicz M. S. (2001) Conductivity measurements of dilute aqueous HCl solutions to high temperatures and pressures using a flow-through cell. *J. Phys. Chem. B* **105**, 1260–1266.

Hoffmann M. M., Darab J. G., Palmer B. J. and Fulton J. L. (1999) A transition in the Ni^{2+} complex structure from six- to four-coordinate upon formation of ion pair species in supercritical water: an X-ray absorption fine structure, near-infrared, and molecular dynamics study. *J. Phys. Chem. A* **103**, 8471–8482.

Hovey J. K., Pitzer K. S., Tanger J. C. I., Bischoff J. L. and Rosenbauer R. J. (1990) Vapor–liquid phase equilibria of potassium chloride-water mixtures: equation-of-state representation for KCl–H_2O and NaCl–H_2O. *J. Phys. Chem.* **94**, 1175–1179.

Irving H. and Williams R. J. P. (1953) The stability of transition-metal complexes. *J. Chem. Soc.*, 3192–3210.

Ito E. and Anderson, Jr., A. T. (1983) Submarine metamorphism of gabbros from the Mid-Cayman Rise: petrographic and mineralogic constraints on hydrothermal processes at slow-spreading ridges. *Contrib. Mineral. Petrol.* **82**, 371–388.

Japas M. L. and Levelt Sengers J. M. H. (1989) Gas solubility and Henry's law near the solvent's critical point. *AlChe J.* **35**, 705–713.

Jupp T. and Schultz A. (2000) A thermodynamic explanation for black smoker temperatures. *Nature* **403**, 880–883.

Kelley D. S. and Delaney J. R. (1987) Two-phase separation and fracturing in mid-ocean ridge gabbros at temperatures greater than 700 °C. *Earth Planet. Sci. Lett.* **83**, 53–66.

Kelley D. S. and Fruh-Green G. L. (2001) Volatile lines of descent in submarine plutonic environments: insights from stable isotope and fluid inclusion analyses. *Geochim. Cosmochim. Acta* **65**, 3325–3346.

Khaibullin I. K. and Borisov N. M. (1965) Phase equilibria in the sodium chloride-water system at high temperatures. *Russ. J. Phys. Chem.* **39**, 361–364 (English translation).

Khaibullin I. K. and Borisov N. M. (1966) Experimental investigation of the thermal properties of aqueous and vapor solutions of sodium and potassium chlorides at phase equilibrium. *Teplofizika Vysokikh Temperatur.* **4**, 489–494 (English translation).

Knauss K. G., Wolery T. J. and Jackson K. J. (1990) A new approach to measuring pH in brines and other concentrated electrolytes. *Geochim. Cosmochim. Acta* **54**, 1519–1523.

Knight C. L. and Bodnar R. J. (1989) Synthetic fluid inclusions: IX. Critical PVTX properties of NaCl–H_2O solutions. *Geochim. Cosmochim. Acta* **53**, 3–8.

Kumagai H., Nakamura K., Toki T., Morishita T., Okino K., Ishibashi J.-I., Tsunogai U., Kawagucci S., Gamo T., Shibuya T., Sawaguchi T., Neo N., Joshima M., Sato T. and Takai K. (2008) Geological background of the Kairei and Edmond hydrothermal fields along the Central Indian Ridge: implications of their vent fluids' distinct chemistry. *Geofluids* **8**, 239–251.

Larson B. I., Lilley M. D. and Olson E. J. (2009) Parameters of subsurface brines and hydrothermal processes 12–15 months after the 1999 magmatic event at the Main Endeavour Field as inferred from in situ time series measurements of chloride and temperature. *J. Geophys. Res.* **144**, B01207. http://dx.doi.org/10.1029/2008JB005627.

Lauher J. W. and Ibers J. A. (1975) Structure of tetramethylammonium tetrachloroferrate(II), $[N(CH_3)_4]_2[FeCl_4]$. Comparison

of iron(II) and Iron(III) bond lengths in high-spin tetrahedral environments. *Inorg. Chem.* **14**, 348–352.

le Roux P. J., Shirey S. B., Hauri E. H., Perfit M. R. and Bender J. F. (2006) The effects of variable sources, processes and contaminants on the composition of northern EPR MORB (8–10°N and 12–14°N): evidence from volatiles (H_2O, CO_2, S) and halogens (F, Cl). *Earth Planet. Sci. Lett.* **251**, 209–231.

Lerchbaumer L. and Audetat A. (2012) High Cu concentrations in vapor-type fluid inclusions: an artifact? *Geochim. Cosmochim. Acta* **88**, 255–274.

Levelt Sengers J. M. H., Everhart C. M., Morrison G. and Pitzer K. S. (1986) Thermodynamic anomalies in near-critical aqueous NaCl solutions. *Chem. Eng. Commun.* **47**, 315–328.

Levelt Sengers J. M. H., Harvey A. H., Crovetto R. and Gallagher J. S. (1992) Standard states, reference states and finite-concentration effects in near-critical mixtures with applications to aqueous solutions. *Fluid Phase Equilib.* **81**, 85–107.

Liebscher A. (2007) Experimental studies in model fluid systems. In *Fluid–Fluid Interactions* (eds. A. Liebscher, C. A. Heinrich). Rev. Mineral. Geochem. 65. MSA, Chantilly, VA. pp. 15–47.

Liebscher A. and Heinrich C. A. (2007) Fluid–fluid interactions in the Earth's lithosphere. In *Fluid–Fluid Interactions* (A. Liebscher, C. A. Heinrich). Rev. Mineral. Geochem. 65. MSA, Chantilly, VA. pp. 1–13.

Liebscher A., Luders V., Heinrich W. and Schettler G. (2006) Br/Cl signature of hydrothermal fluids: liquid–vapour fractionation of bromine revisited. *Geofluids* **6**, 113–121.

Lilley M. D., Lupton J. E., Butterfield D. A. and Olson E. (2003) Magmatic events can produce rapid changes in hydrothermal vent chemistry. *Nature* **422**, 878–881.

Liu B., Oscarson J. L., Peterson C. J. and Izatt R. M. (2006) Improved thermodynamic model for aqueous NaCl solutions from 350 to 400 °C. *Ind. Eng. Chem. Res.* **45**, 2929–2939.

Liu W., Borg S. J., Testemale D., Etschmann B., Hazemann J.-L. and Brugger J. (2011) Speciation and thermodynamic properties for cobalt chloride complexes in hydrothermal fluids at 35–400 °C and 600 bar: an in-situ XAS study. *Geochim. Cosmochim. Acta* **75**, 1227–1248.

Majer V., Hui L., Crovetto R. and Wood R. H. (1991) Volumetric properties of aqueous 1–1 electrolyte solutions near and above the critical temperature of water I. Densities and apparent molar volumes of NaCl(aq) from 0.0025 $mol*kg^{-1}$ to 3.1 $mol*kg^{-1}$, 604.4 K to 725.5 K, and 18.5 MPa to 38.0 MPa. *J. Chem. Thermodyn.* **23**, 213–229.

Marcus Y. (1988) Ionic radii in aqueous solutions. *Chem. Rev.* **88**, 1475–1498.

Marshall W. L. (1990) Critical curves of aqueous electrolytes related to ionization behaviour: new temperatures for sodium chloride solutions. *J. Chem. Soc. Faraday Trans.* **86**, 1807–1814.

Mei Y., Liu W., Sherman D. M. and Brugger J. (2014) Metal complexation and ion hydration in low density hydrothermal fluids: Ab initio molecular dynamics simulation of Cu(I) and Au(I) in chloride solutions (25–1000 °C, 1–5000 bar). *Geochim. Cosmochim. Acta* **131**, 196–212.

Mesmer R. E., Marshall W. L., Palmer D. A., Simonson J. M. and Holmes H. F. (1988) Thermodynamics of aqueous association and ionization reactions at high temperatures and pressures. *J. Sol. Chem.* **17**, 699–718.

Michael P. J. and Cornell W. C. (1998) Influence of spreading rate and magma supply on crystallization and assimilation beneath mid-ocean ridges: evidence from chlorine and major element chemistry of mid-ocean ridge basalts. *J. Geophys. Res.* **103**, 18325–18356.

Michard G., Albarede F., Michard A., Minster J.-F., Charlou J.-L. and Tan N. (1984) Chemistry of solutions from the 13°N East Pacific Rise hydrothermal site. *Earth Planet. Sci. Lett.* **67**, 297–307.

Migdisov A. A., Zezin D. and Williams-Jones A. E. (2011) An experimental study of cobalt (II) complexation in Cl^- and H_2S-bearing hydrothermal solutions. *Geochim. Cosmochim. Acta* **75**, 4065–4079.

Mottl M. J. and Holland H. D. (1978) Chemical exchange during hydrothermal alteration of basalt by seawater I. Experimental results for major and minor components of seawater. *Geochim. Cosmochim. Acta* **42**, 1103–1115.

Mottl M. J., Seewald J. S., Wheat C. G., Tivey M. K., Michael P. J., Proskurowski G., McCollom T. M., Reeves E., Sharkey J., You C.-F., Chan L.-H. and Pichler T. (2011) Chemistry of hot springs along the Eastern Lau Spreading Center. *Geochim. Cosmochim. Acta* **75**, 1013–1038.

Nagaseki H. and Hayashi K. (2008) Experimental study of the behavior of copper and zinc in a boiling hydrothermal system. *Geology* **36**, 27–30.

Nehlig P. (1991) Salinity of oceanic hydrothermal fluids: a fluid inclusion study. *Earth Planet. Sci. Lett.* **102**, 310–325.

Norton D. L. (1984) Theory of hydrothermal systems. *Ann. Rev. Earth Planet. Sci.* **12**, 155–177.

Oelkers E. H. and Helgeson H. C. (1993) Multiple ion association in supercritical aqueous solutions of single electrolytes. *Science* **261**, 888–891.

Oosting S. E. and Von Damm K. L. (1996) Bromide/chloride fractionation in seafloor hydrothermal fluids from 9–10°N East Pacific Rise. *Earth Planet. Sci. Lett.* **144**, 133–145.

Oscarson J. L., Liu B. and Izatt R. M. (2004) A model incorporating ion dissociation, solute concentration, and solution density effects to describe the thermodynamics of aqueous sodium chloride solutions in the critical region of water. *Ind. Eng. Chem. Res.* **43**, 7635–7646.

Palmer D. A., Simonson J. M. and Jensen J. P. (2004) Partitioning of electrolytes to steam and their solubilities in steam. In *Aqueous Systems at Elevated Temperatures and Pressures: Physical Chemistry in Water, Steam and Hydrothermal Solutions* (eds. D. A. Palmer, R. Fernandez-Prini and A. H. Harvey). Elsevier, San Diego, pp. 409–439.

Pester N. J., Rough M., Ding K. and Seyfried, Jr., W. E. (2011) A new Fe/Mn geothermometer for hydrothermal systems: implications for high-salinity fluids at 13°N on the East Pacific Rise. *Geochim. Cosmochim. Acta* **75**, 7881–7892.

Pester N. J., Reeves E. P., Rough M. E., Ding K., Seewald J. S. and Seyfried, Jr., W. E. (2012) Subseafloor phase equilibria in high-temperature hydrothermal fluids of the Lucky Strike Seamount (Mid-Atlantic Ridge, 37°17′N). *Geochim. Cosmochim. Acta* **90**, 303–322.

Pester N. J., Ding K. and Seyfried, Jr., W. E. (2014a) Magmatic eruptions and iron volatility in deep-sea hydrothermal fluids. *Geology* **42**, 255–258.

Pester N. J., Schaen A. T., Ding K. and Seyfried, Jr., W. E. (2014b) Experimental constraints on hydrothermal circulation in mid-ocean ridges. *Goldschmid. Abstr.*, 1943.

Pitzer K. S. (1977) Electrolyte theory: improvements since Debye and Hückel. *Accounts Chem. Res.* **10**, 371–377.

Pitzer K. S. and Jiang S. Y. (1996) Equation of state for NaCl–H_2O: comparison with mineral dehydration equilibria. *Contrib. Mineral. Petrol.* **122**, 428–430.

Pokrovski G. S., Roux J. and Harrichoury J. (2005) Fluid density control on vapor–liquid partitioning of metals in hydrothermal systems. *Geology* **33**, 657–660.

Pokrovski G. S., Borisova A. Y. and Harrichoury J. (2008) The effect of sulfur on the vapor–liquid fractionation of metals in hydrothermal systems. *Earth Planet. Sci. Lett.* **266**, 345–362.

Pokrovski G. S., Borisova A. Y. and Bychkov A. Y. (2013) Speciation and transport of metals and metalloids in geological vapors. In *Thermodynamics of Geothermal Fluids* (eds. A. Stefansson, T. Driesner, P. Benezeth). Rev. Mineral. Geochem. 76. MSA, Chantilly, VA. pp. 165–218.

Reeves E. P., Seewald J. S., Saccocia P. J., Bach W., Craddock P. R., Shanks W. C., Sylva S. P., Walsh E., Pichler T. and Rosner M. (2011) Geochemistry of hydrothermal fluids from the PACMANUS, Northeast Pual and Vienna Woods hydrothermal fields, Manus Basin, Papua New Guinea. *Geochim. Cosmochim. Acta* **75**, 1088–1123.

Rempel K. U., Liebscher A., Meixner A., Romer R. L. and Heinrich W. (2012) An experimental study of the elemental and isotopic fractionation of copper between aqueous vapour and liquid to 450 °C and 400 bar in the CuCl–NaCl–H_2O and CuCl–NaHS–NaCl–H_2O systems. *Geochim. Cosmochim. Acta* **94**, 199–216.

Rice D. W. and Gregory N. W. (1968) Vaporization equilibria in the sodium chloride-zinc chloride system. *J. Phys. Chem.* **72**, 4524–4528.

Rosenbauer R. J. and Bischoff J. L. (1987) Pressure-composition relations for coexisting gases and liquids and the critical points in the system NaCl–H_2O at 450, 475, and 500 °C. *Geochim. Cosmochim. Acta* **51**, 2349–2354.

Saccocia P. J. and Gillis K. M. (1995) Hydrothermal upflow zones in the oceanic crust. *Earth Planet. Sci. Lett.* **136**, 1–16.

Schmidt K., Koschinsky A., Garbe-Schonberg D., de Carvalho L. M. and Seifert R. (2007) Geochemistry of hydrothermal fluids from the ultramafic-hosted Logatchev hydrothermal field, 15°N on the Mid-Atlantic Ridge: temporal and spatial investigation. *Chem. Geol.* **242**, 1–21.

Sedlbauer J. and Wood R. H. (2004) Thermodynamic properties of dilute NaCl(aq) solutions near the critical point of water. *J. Phys. Chem. B* **108**, 11838–11849.

Seewald J. S. and Seyfried, Jr., W. E. (1990) The effect of temperature on metal mobility in subseafloor hydrothermal systems: constraints from basalt alteration experiments. *Earth Planet. Sci. Lett.* **101**, 388–403.

Seewald J., Cruse A. and Saccocia P. (2003) Aqueous volatiles in hydrothermal fluids from the Main Endeavour Field, northern Juan de Fuca Ridge: Temporal variability following earthquake activity. *Earth Planet. Sci. Lett.* **216**, 575–590.

Seward T. M. and Barnes H. L. (1997) Metal transport by hydrothermal ore fluids. In *Geochemistry of Hydrothermal Ore Deposits, 3rd* (ed. H. L. Barnes). John Wiley and Sons Inc. pp. 435–486.

Seward T. M. and Driesner T. (2004) Hydrothermal solution structure: experiments and computer simulations. In *Aqueous Systems at Elevated Temperatures and Pressures: Physical Chemistry in Water, Steam and Hydrothermal Solutions* (eds. D. A. Palmer, R. Fernandez-Prini and A. H. Harvey). Elsevier, San Diego, pp. 149–182.

Seward T. M., Henderson C. M. B., Charnock J. M. and Driesner T. (1999) An EXAFS study of solvation and ion pairing in aqueous strontium solutions to 300 °C. *Geochim. Cosmochim. Acta* **63**, 2409–2418.

Seyfried, Jr., W. E. and Shanks, III, W. C. (2004) Alteration and mass transport in mid-ocean ridge hydrothermal systems: controls on the chemical and isotopic evolution of high-temperature crustal fluids. In *Hydrogeology of the Oceanic Lithosphere* (eds. E. Davis and H. Elderfield). Cambridge University Press, Cambridge, pp. 451–495.

Seyfried W. E., Jr., Ding K. and Rao B. (2002) Experimental calibration of metastable plagioclase-epidote-fluid equilibria at elevated temperatures and pressures: applications to the chemistry of hydrothermal fluids at mid-ocean ridges. In *Water–Rock Interactions, Ore Deposits and Environmental Geochemistry: A Tribute to David A. Crerar* (eds. R. Hellman, S. A. Wood). Geochem. Soci., Spec. Pub., 7, St. Louis. pp. 257–278.

Seyfried, Jr., W. E., Seewald J. S., Berndt M. E., Ding K. and Foustoukos D. I. (2003) Chemistry of hydrothermal vent fluids from the Main Endeavour Field, Northern Juan de Fuca Ridge: Geochemical controls in the aftermath of June 1999 seismic events. *J. Geophys. Res.* **108**, 2429, doi:2410.1029/2002JB001957.

Seyfried, Jr., W. E., Pester N. J., Ding K. and Rough M. (2011) Vent fluid chemistry of the Rainbow hydrothermal system (36°N, MAR): Phase equilibria and in-situ pH controls on subseafloor alteration processes. *Geochim. Cosmochim. Acta* **75**, 1574–1593.

Shadle S. E., Hedman B., Hodgson K. O. and Solomon E. I. (1995) Ligand K-edge X-ray absorption spectroscopic studies: metal-ligand covalency in a series of transition metal tetrachlorides. *J. Am. Chem. Soc.* **117**, 2259–2272.

Shmulovich K. I., Landwehr D., Simon K. and Heinrich W. (1999) Stable isotope fractionation between liquid and vapour in water-salt systems up to 600 °C. *Chem. Geol.* **157**, 343–354.

Shock E. L., Oelkers E. H., Sverjensky D. A., Johnson J. W. and Helgeson H. C. (1992) Calculation of thermodynamic and transport properties of aqueous species at high pressures and temperatures. Effective electrostatic radii, dissociation constants and standard partial molal properties to 1000 °C and 5 kb. *J. Chem. Soc. London, Faraday Trans.* **88**, 803–826.

Simon A. C., Pettke T., Candela P. A., Piccoli P. M. and Heinrich C. A. (2004) Magnetite solubility and iron transport in magmatic-hydrothermal environments. *Geochim. Cosmochim. Acta* **68**, 4905–4914.

Simonson J. M. and Palmer D. A. (1993) Liquid–vapor partitioning of HCl(aq) to 350 °C. *Geochim. Cosmochim. Acta* **57**, 1–7.

Sourirajan S. and Kennedy G. C. (1962) The system H_2O–NaCl at elevated temperatures and pressures. *Am. J. Sci.* **260**, 115–141.

Susak N. J. and Crerar D. A. (1985) Spectra and coordination changes of transition metals in hydrothermal solutions: implications for ore genesis. *Geochim. Cosmochim. Acta* **49**, 555–564.

Syverson D. D., Pester N. J., Craddock P. R. and Seyfried, Jr., W. E. (2014) Fe isotope fractionation during phase separation in the NaCl–H_2O system: an experimental study with implications for seafloor hydrothermal systems. *Earth Planet. Sci. Lett.* **406**, 223–232.

Tanger, IV, J. C. and Helgeson H. C. (1988) Calculation of the thermodynamic and transport properties of aqueous species at high pressures and temperatures: revised equations of state for the standard partial molal properties of ions and electrolytes. *Am. J. Sci.* **288**, 19–98.

Testemale D., Brugger J., Liu W., Etschmann B. and Hazemann J.-L. (2009) In-situ X-ray absorption study of Iron(II) speciation in brines up to supercritical conditions. *Chem. Geol.* **264**, 295–310.

Trommsdorff V. and Skippen G. (1986) Vapour loss ("boiling") as a mechanism for fluid evolution in metamorphic rocks. *Contrib. Mineral. Petrol.* **94**, 317–322.

Vanko D. A. (1986) High-chlorine amphiboles from oceanic rocks: product of highly-saline hydrothermal fluids? *Am. Mineral.* **71**, 51–59.

Vanko D. A. and Laverne C. (1998) Hydrothermal an orthitization of plagioclase within the magmatic/hydrothermal transition at mid-ocean ridges: examples from deep sheeted dikes (Hole 504B, Costa Rica Rift) and a sheeted dike root zone (Oman ophiolite). *Earth Planet. Sci. Lett.* **162**, 27–43.

Vanko D. A., Bach W., Roberts S., Yeats C. J. and Scott S. D. (2004) Fluid inclusion evidence for subsurface phase separation

and variable mixing regimes beneath the deep-sea PACMANUS hydrothermal field, Manus Basin back arc rift, Papua New Guinea. *J. Geophys. Res.*, B03201.

Von Damm K. L. (2000) Chemistry of hydrothermal vent fluids from 9°-10°N, East Pacific Rise: "Time zero", the immediate posteruptive period. *J. Geophys. Res.* **105**, 11203–11222.

Von Damm K. L. (2004) Evolution of the hydrothermal system at East Pacific Rise 9°50′N: geochemical evidence for changes in the upper oceanic crust. In *Mid-Ocean Ridges: Hydrothermal Interactions Between the Lithosphere and Oceans* (eds. C. R. German, J. Lin, L. M. Parson). Geophys. Monogr. Ser., 148. AGU, Washington, DC. pp. 285–305.

Von Damm K. L., Edmond J. M., Grant B., Measures C. I., Walden B. and Weiss R. F. (1985a) Chemistry of submarine hydrothermal solutions at 21°N, East Pacific Rise. *Geochim. Cosmochim. Acta* **49**, 2197–2220.

Von Damm K. L., Edmond J. M., Measures C. I. and Grant B. (1985b) Chemistry of submarine hydrothermal solutions at Guaymas Basin, Gulf of California. *Geochim. Cosmochim. Acta* **49**, 2221–2237.

Von Damm K. L., Bray A. M., Buttermore L. G. and Oosting S. E. (1998) The geochemical controls on vent fluids from Lucky Strike vent field, Mid-Atlantic Ridge. *Earth Planet. Sci. Lett.* **160**, 521–536.

Von Damm K. L., Parker C. M., Gallant R. M. and Loveless J. P. (2002) Chemical evolution of hydrothermal fluids from EPR 21 N: 23 years later in a phase separating world. Eos. *Trans. Am. Geophys. Union* **83**.

White D. E., Wood R. H. and Biggerstaff D. R. (1988) Heat capacities of 0.0150 mol*kg^{-1} NaCl(aq) from 604 to 718 K at 32 MPa. *J. Chem. Thermodyn.* **20**, 159–168.

Wiesner J. R., Srivastava R. C., Kennard C. H. L., DiVaira M. and Lingafelter E. C. (1967) The crystal structures of tetramethylammonium tetrachloro-cobaltate (II), -nickelate (II), and -zincate (II). *Acta Cryst.* **23**, 565–574.

Williams-Jones A. E., Migdisov A. A., Archibald S. M. and Xiao Z. (2002) Vapor-transport of ore metals. In *Water–Rock Interactions, Ore Deposits, and Environmental Geochemistry: A Tribute to David A. Crerar* (eds. R. Hellman and S. A. Wood). The Geochemical Society, St Louis, MO.

Associate editor: Gleb S. Pokrovski